serum IL-18 was increased dramatically at the late phase. In the present study, we investigated the involvement of IL-18 in the liver injury and focused on the interactions among IL-18 and NKT cells, neutrophils, macrophages, and monocytes, which play important roles in various diseases. The results obtained provide new insights into the inflammatory network among macrophages, neutrophils, and NKT cells during liver injury.

MATERIALS AND METHODS

Mice

Vα14 NKT KO mice were generated as described [7], and C57BL/6 mice were purchased from Japan SLC (Shizuoka, Japan). All animals were housed in pathogen-free rooms under strict barrier conditions and received humane care according to the guidelines of the Animal Care Committees of Gifu University School of Medicine (Gifu, Japan) and Tokyo Metropolitan Institute of Medical Science (Tokyo, Japan).

Antibodies

Mice were injected i.v. with 100 μg αCD40 [16] or 100 μg purified rat IgG2a as a control (BD PharMingen, San Diego, CA, USA). In addition, some mice were injected i.p. (200 μg/mouse) at Days −1, +1, and +3 with a rat mAb against mouse Gr-1 (clone RB6-8C5) and control rat IgG2b (both from eBioscience, San Diego, CA, USA). At Days −1, +1, and +3, other mice were injected i.p. with a rat anti-mouse IL-18 mAb (50 μg/mouse) and rat IgG (both from MBL, Nagoya, Japan).

Cell isolation

To isolate IHLs, single-cell suspensions were prepared from liver perfused with PBS via the inferior vena cava and digested in 10 mL RPMI 1640 (Life Technologies, Gaithersburg, MD, USA) containing 0.02% (wt/vol) collagenase IV (Sigma-Aldrich, St. Louis, MO, USA) and 0.002% (wt/vol) DNase I (Sigma-Aldrich) for 40 min at 37°C. Cells were overlaid on Lympholyte M (Cedarlane, Westbury, NY, USA) in PBS. Bone marrow cells were collected from the femurs and tibias of mice. To isolate PBMCs, peripheral blood (0.4 mL) was obtained by cardiac puncture under ether anesthesia. After density separation, cell counts and immunofluorescence analyses were performed.

Tissue RNA analyses

Frozen livers were mechanically pulverized under liquid nitrogen, and total RNAs were isolated for RPAs as described previously [15]. All reagents for the RPAs were purchased from BD PharMingen.

ELISA

The serum IL-18, TNF-α, and IFN-γ concentrations were assayed using specific ELISA kits (IL-18, MBL; TNF-α and IFN-γ, Genzyme Techne Corp., Minneapolis, MN, USA), according to each corresponding manufacturer's protocols.

Immunohistochemistry

The samples were embedded in OCT compound (Tissue Tek, Miles, Elkhart, IN, USA) and frozen in liquid nitrogen. Sections were cut at 4 μm thickness using a cryostat and fixed with cold acetone for 10 min. The fixed sections were treated with rat anti-mouse F4/80, Ly-6C, and Gr-1 mAb (10 μg/mL), followed by a streptavidin-biotin-HRP complex (Dako, Glostrup, Denmark). The positive reactions were visualized with 0.035% H_2O_2 and 0.03% 3,3′-diaminobenzidine (Wako, Tokyo, Japan) in 50 mM Tris-HCl (pH 7.6) for 2–3 min. After 4% formaldehyde fixation, the stained sections were counterstained with hematoxylin and subjected to microscopic observation.

Flow cytometry

The cells were surface-stained with fluorochrome-conjugated mAb for 20 min on ice. The following antibodies were used: anti-CD3, anti-NK1.1, anti-CD11b, and anti-CD11c (all from eBioscience). The F4/80 and Ly-6C mAb (BMA Biomedicals, Geneva, Switzerland) were also used. In addition, the cells were surface-stained with FITC-conjugated anti-CD3, FITC-conjugated anti-CD11b, and allophycocyanin-conjugated anti-NK1.1 mAb, together with anti-IFN-γ-PE and anti-TNF-α-PE mAb (all from BD PharMingen) for intracellular cytokine detection. Samples were acquired using a FACSCalibur flow cytometer, and data were analyzed using the CellQuest software (BD Immunocytometry Systems, San Jose, CA, USA) and FlowJo software (Tree Star, San Carlos, CA, USA).

BrdU incorporation

For in vivo BrdU labeling, mice received a 100-μL i.p. injection of a 10-mg/mL solution of BrdU in PBS at 2 h before sacrifice. Single-cell suspensions of IHLs were prepared at 24 h after αCD40 injection and surface-stained with PE-CD11b. Following the surface staining, the cells were fixed, stained for intracellular BrdU using a FITC-BrdU flow kit (BD PharMingen), and analyzed by flow cytometry.

Data analysis

All data are expressed as the mean + SD. Values of $P < 0.05$ were considered statistically significant.

RESULTS

A single injection of αCD40 increases serum IL-18

We found that the serum ALT activity began to elevate on Day 1 and was clearly increased on Day 5 after αCD40 injection. We confirmed further that inflammatory cytokine and chemokine mRNA expressions were increased at Days 1 and 5 in C57BL/6 mice (Supplemental Fig. 1A). We measured the serum IL-18 level and found that it began to increase at Day 3 and was remarkably increased until Day 5 after the injection. To determine the infiltration of inflammatory cells in the same livers, we counted the absolute number of IHLs and calculated the number of cells in each IHL subset. As shown in **Fig. 1B**, Gr-1^{++}/CD$11b^{+}$ cells (mostly neutrophils) were increased until Day 1 and then decreased at Days 3 and 5. On the other hand, Gr-1^{+}/CD$11b^{+}$ cells (mostly macrophages and monocytes) were increased and reached a peak at Day 3 and then decreased until Day 5. Furthermore, to evaluate the numbers of macrophages and their precursors in the liver, the cells were stained with the CD11b, F4/80, and Ly-6C mAb, which recognize antigens on macrophages and their precursors at different stages of differentiation [17]. The numbers of Ly-$6C^{++}$/CD$11b^{+}$ cells (mostly monocytes) and F4/80^{+}/CD$11b^{+}$ cells (tissue macrophages) began to increase by Day 1, reached a peak at Day 3, and then decreased until Day 5. In immunohistochemical analyses, Gr-1^{+} cells were increased at Day 1 in the liver parenchyma, whereas Ly-$6C^{+}$ and F4/80^{+} cells were increased at Day 3 in the liver (Fig. 1C), consistent with the FACS data.

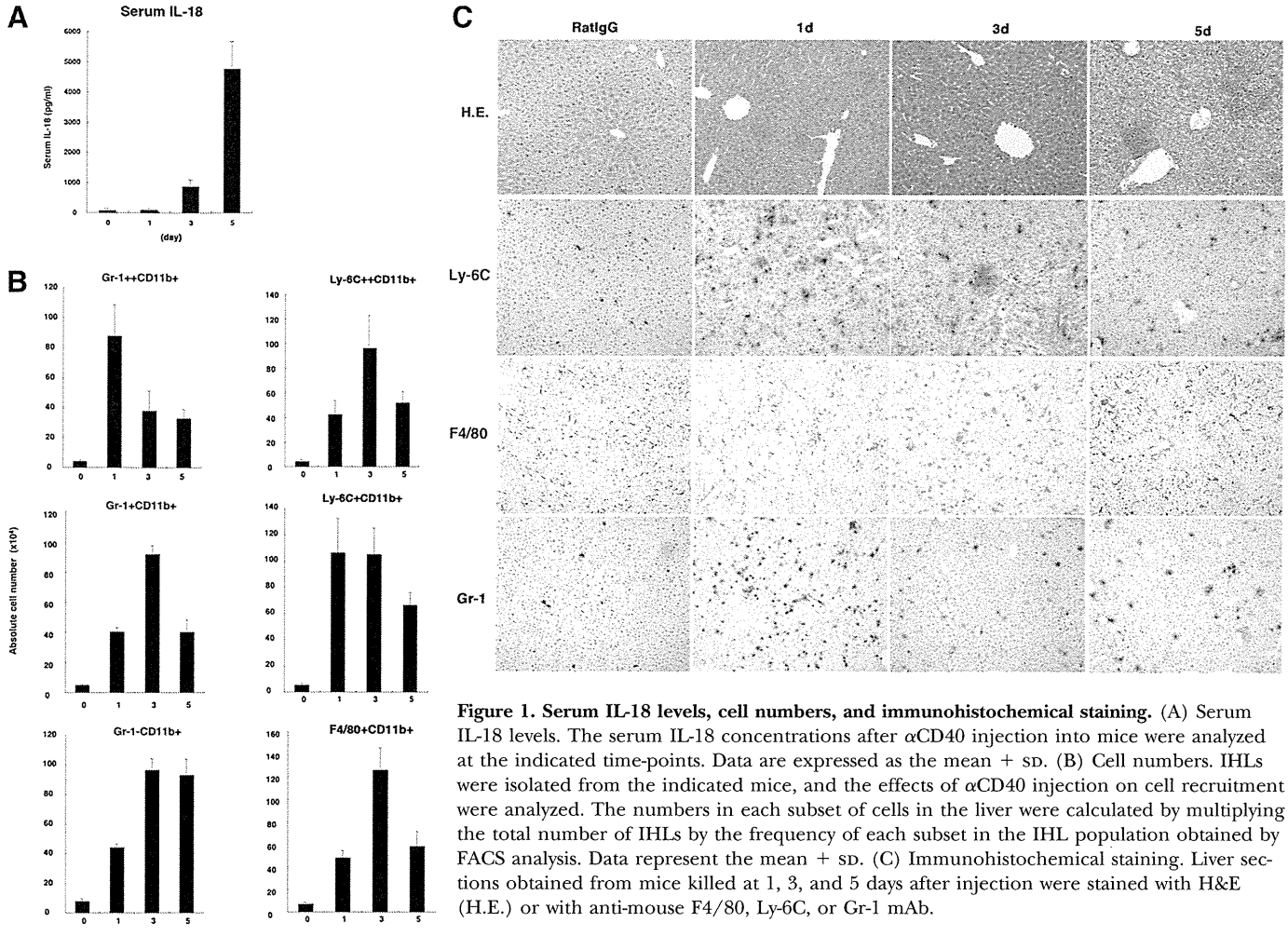

Figure 1. Serum IL-18 levels, cell numbers, and immunohistochemical staining. (A) Serum IL-18 levels. The serum IL-18 concentrations after αCD40 injection into mice were analyzed at the indicated time-points. Data are expressed as the mean + SD. (B) Cell numbers. IHLs were isolated from the indicated mice, and the effects of αCD40 injection on cell recruitment were analyzed. The numbers in each subset of cells in the liver were calculated by multiplying the total number of IHLs by the frequency of each subset in the IHL population obtained by FACS analysis. Data represent the mean + SD. (C) Immunohistochemical staining. Liver sections obtained from mice killed at 1, 3, and 5 days after injection were stained with H&E (H.E.) or with anti-mouse F4/80, Ly-6C, or Gr-1 mAb.

Proliferation and differentiation of macrophages after αCD40 injection

As reported previously [14], macrophages were key players in this liver injury. We confirmed that αCD11b mAb treatment suppressed inflammatory cytokine and chemokine expressions in the liver and the serum IL-18 levels (Supplemental Fig. 2A and B), indicating that macrophages are IL-18 producers, consistent with a previous report [11].

Next, to evaluate the function of macrophages after αCD40 injection, we analyzed the proliferation of macrophages by BrdU staining in the liver, bone marrow, and PBMCs. We injected 2 mg BrdU i.p. into mice at 2 h before sacrifice. Proliferation of $CD11b^+$ cells peaked in each tissue at Day 3 after injection and decreased by Day 5 (**Fig. 2A**), consistent with the numbers of the macrophage populations in the FACS analysis.

To determine whether differentiation from monocytes to tissue macrophages was induced in each tissue, we investigated the changes in the proportions of $Ly\text{-}6C^+$ and $F4/80^+$ cells among the $CD11b^+$ cells (Fig. 2B). $Ly\text{-}6C^-/F4/80^+/CD11b^+$ and $Ly\text{-}6C^+/F4/80^-/CD11b^+$ cells comprised the majority of cells in the liver after injection of the control antibody, and $Ly\text{-}6C^+/F4/80^+/CD11b^+$ cells increased at Day 1 and peaked at Day 3. These findings demonstrate that the proportion of $Ly\text{-}6C^-/F4/80^+/CD11b^+$ cells increased from Days 3 to 5, indicating that differentiation from monocytes to tissue macrophages had occurred by Day 3. In the bone marrow, $Ly\text{-}6C^+/F4/80^+/CD11b^+$ cells began to increase at Day 1 after αCD40 injection compared with the findings for the control antibody but had decreased by Day 5, indicating that αCD40 stimulation also induced the differentiation of macrophages. Similarly, $Ly\text{-}6C^+/F4/80^+/CD11b^+$ cells, among the PBMCs, began to increase by Day 1 after αCD40 injection and peaked at Day 3.

Role of NKT cells

To evaluate the role of NKT cells in this liver injury, NKT KO and C57BL/6 mice were injected with αCD40 and killed at Days 1 and 5. No significant difference between the serum ALT activities was observed after rat IgG injection, which is presented as Day 0, and NKT KO mice exhibited significantly lower serum ALT activities than WT mice at Days 1 and 5 ($P<0.05$; **Fig. 3A**). We also found that the absolute numbers of NK cells, T cells, macrophages, and neutrophils among the IHLs were reduced significantly in NKT KO mice (Fig. 3B). Consistent with the reduced number of IHLs in NKT KO mice, the IFN-γ, TNF-α, CCL2, and CCL5 mRNA expressions in the liver were suppressed at Days 1 and 5 after αCD40 injection (Fig. 3C and

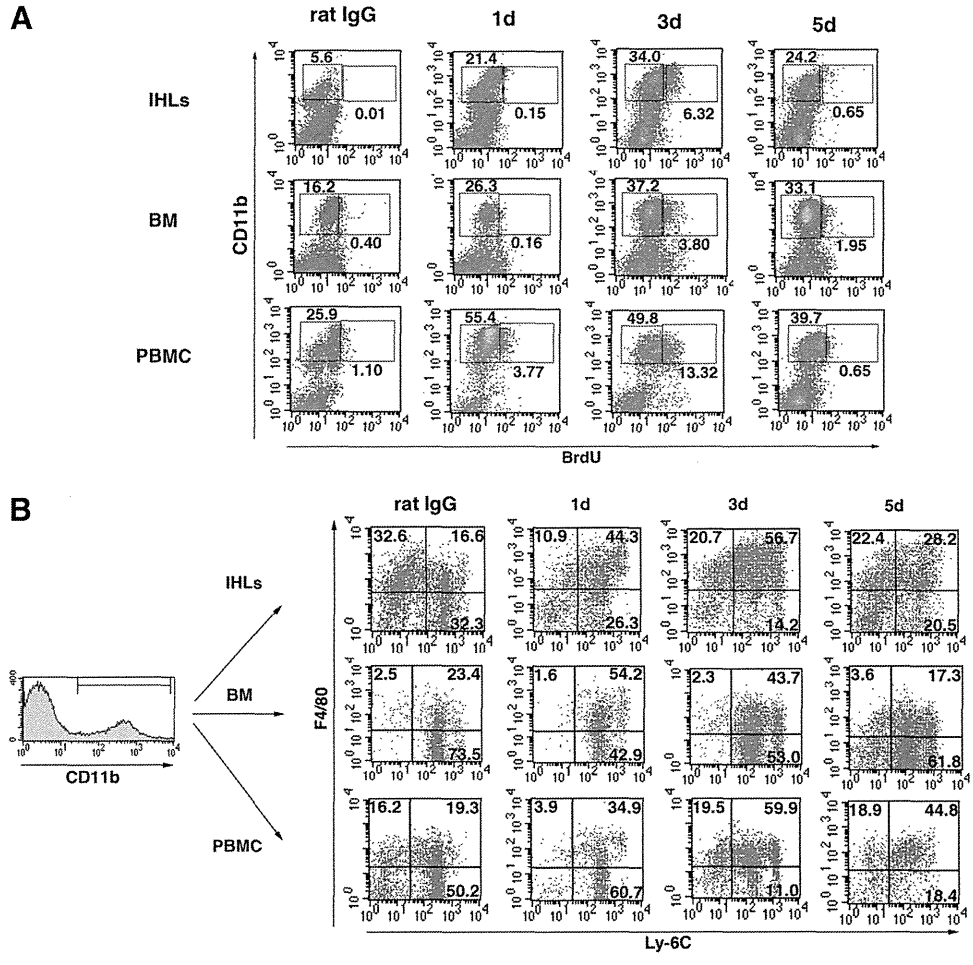

Figure 2. Macrophage differentiation and proliferation after αCD40 injection. (A) To analyze macrophage proliferation in IHLs, bone marrow (BM), and PBMCs after αCD40 injection, C57BL/6 mice were injected i.p. with 2 mg BrdU at 2 h before sacrifice. Cells were stained with anti-CD11b-allophycocyanin and anti-BrdU-FITC antibodies. (B) To analyze macrophage differentiation in IHLs, bone marrow, and PBMCs, cells were stained with anti-CD11b-allophycocyanin, anti-mouse F4/80-FITC, and anti-mouse Ly-6C-PE mAb.

D). We further found that the IFN-γ production by NK cells and TNF-α production by macrophages were suppressed in NKT KO mice (**Supplemental Fig. 3**). Furthermore, the serum IL-18 levels were reduced in NKT KO mice at Day 5 but not Day 1.

Finally, the numbers of Ly-6C^{++}/CD11b^{+}, Ly-6C^{+}/CD11b^{+}, and F4/80^{+}/CD11b^{+} cells in NKT KO mice were reduced significantly compared with WT mice at Day 5 after injection (Fig. 3E), demonstrating that NKT cells were involved in the macrophage and monocyte infiltration in the liver.

Depletion of neutrophils exacerbates the liver injury

To determine whether neutrophils play a role in this liver injury, we injected αCD40 into C57BL/6 mice with αGr-1 mAb or rat IgG2b at Days −1, +1, and +3. The mice were killed at Day 5. We confirmed that αGr-1 mAb treatment specifically depleted IHLs with an efficiency of >95% (Gr-1^{++}/CD11b^{+} cells), as evaluated by FACS analysis (Supplemental Fig. 4).

Administration of αGr-1 mAb significantly increased the serum ALT activity at Day 5 compared with the control antibody (P<0.05; **Fig. 4A**). Although the total number of IHLs decreased after αCD40 plus αGr-1 mAb treatment, the numbers of Gr-1^{+}/CD11b^{+} cells, including Ly-6C^{++}/CD11b^{+} and F4/80^{+}/CD11b^{+} cells, increased (Fig. 4B, C, and E). Immunohistochemical analyses revealed that Ly-6C^{+} and F4/80^{+} cells were increased in the liver at Day 5 after αCD40 mAb plus αGr-1 mAb treatment (Fig. 4F). Consistent with these observations, the serum TNF-α and IL-18 but not IFN-γ levels were elevated in the neutrophil-depleted state (Fig. 4D). In addition, TNF-α production by Ly-6C^{++}/CD11b^{+} and F4/80^{+}/CD11b^{+} cells was increased in αGr-1 mAb-treated mice (Fig. 4G), suggesting that neutrophils may play a suppressive role in macrophage recruitment and function in this liver inflammation.

Neutralization of IL-18 suppresses the liver injury

To assess whether IL-18 is responsible for the αCD40-induced liver injury, we injected C57BL/6 mice with αIL-18 mAb or rat IgG as a control at –1, +1, and 2 days after αCD40 injection and then killed the mice at Day 5. Administration of αIL-18 mAb significantly suppressed the serum ALT activity at Day 5 (P<0.05; **Fig. 5A**), demonstrating that IL-18 contributes to the liver injury. Consistent with this finding, αIL-18 mAb treatment decreased the IFN-γ and TNF-α mRNA expressions in the liver (Fig. 5B). We also found that αIL-18 mAb treatment inhibited the recruitment of macrophage subpopulations, neutrophils, NK cells, and T cells but not NKT cells into the liver (Fig. 5C). Immunohistochemical analyses revealed that Ly-6C^{+} and F4/80^{+} cells

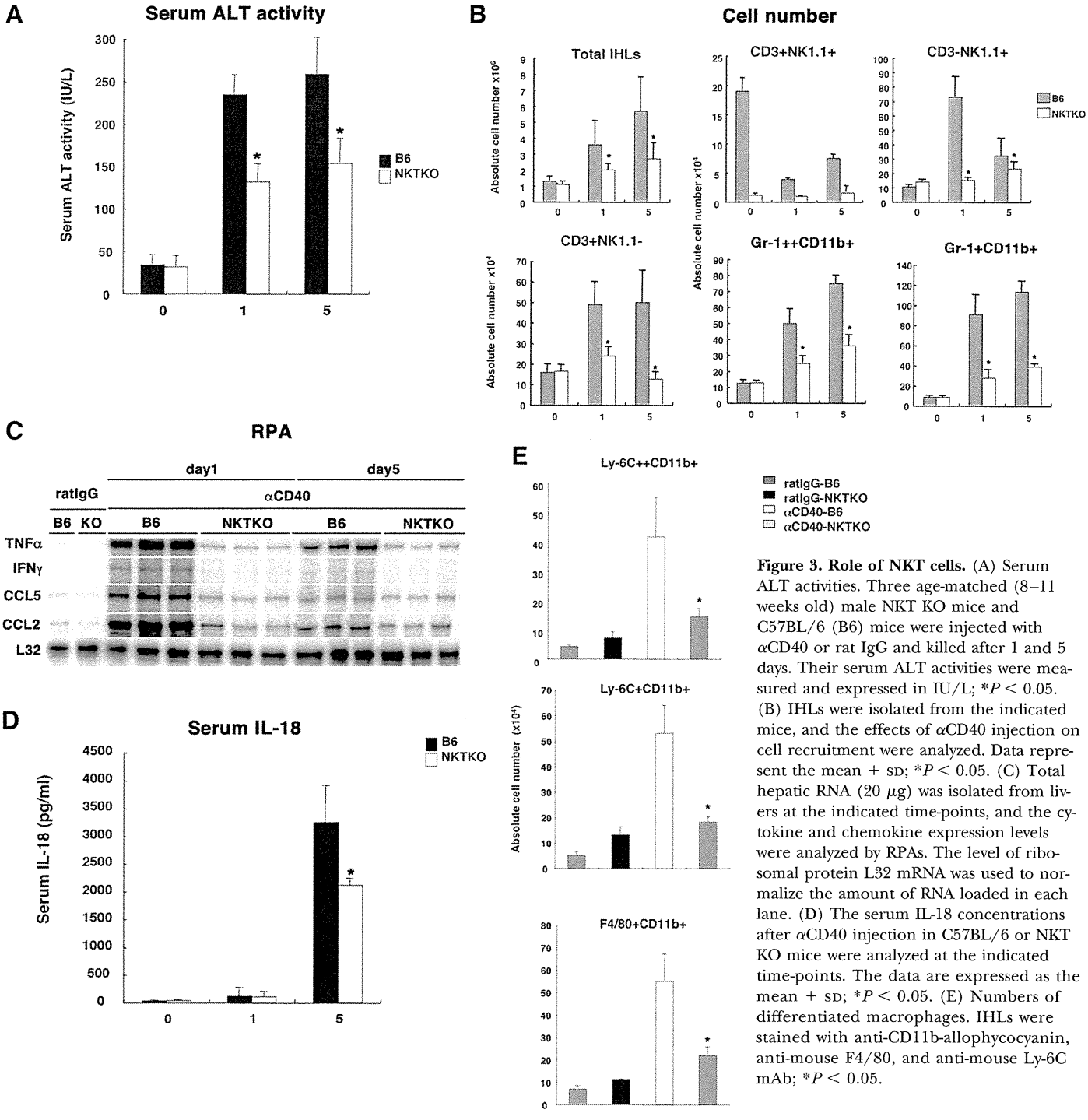

Figure 3. Role of NKT cells. (A) Serum ALT activities. Three age-matched (8–11 weeks old) male NKT KO mice and C57BL/6 (B6) mice were injected with αCD40 or rat IgG and killed after 1 and 5 days. Their serum ALT activities were measured and expressed in IU/L; $*P < 0.05$. (B) IHLs were isolated from the indicated mice, and the effects of αCD40 injection on cell recruitment were analyzed. Data represent the mean + SD; $*P < 0.05$. (C) Total hepatic RNA (20 μg) was isolated from livers at the indicated time-points, and the cytokine and chemokine expression levels were analyzed by RPAs. The level of ribosomal protein L32 mRNA was used to normalize the amount of RNA loaded in each lane. (D) The serum IL-18 concentrations after αCD40 injection in C57BL/6 or NKT KO mice were analyzed at the indicated time-points. The data are expressed as the mean + SD; $*P < 0.05$. (E) Numbers of differentiated macrophages. IHLs were stained with anti-CD11b-allophycocyanin, anti-mouse F4/80, and anti-mouse Ly-6C mAb; $*P < 0.05$.

were decreased in the liver at Day 5 after αCD40 mAb plus αIL-18 mAb treatment (Fig. 5D).

IL-18 causes severe liver injury with high levels of IFN-γ

To evaluate the effect of IL-18 on the late-phase liver injury, we i.p.-injected mice with 1 μg murine rIL-18 at 4 days after αCD40 injection and measured their serum ALT activity and inflammatory cytokine levels. The serum ALT activity was increased significantly by about four times after rIL-18 treatment compared with the control, although the number of IHLs, except for the macrophage population, was suppressed (**Fig. 6A–C**). In addition, serum IFN-γ was elevated significantly after injection of αCD40 with rIL-18, and NK cells strongly produced IFN-γ after rIL-18 treatment (Fig. 6D and E). In contrast, no difference was seen for TNF-α production by macrophages (Fig. 6E). Thus, IL-18 mainly activated NK cells and reduced the numbers of monocytes and neutrophils in the liver (Fig. 6A and B).

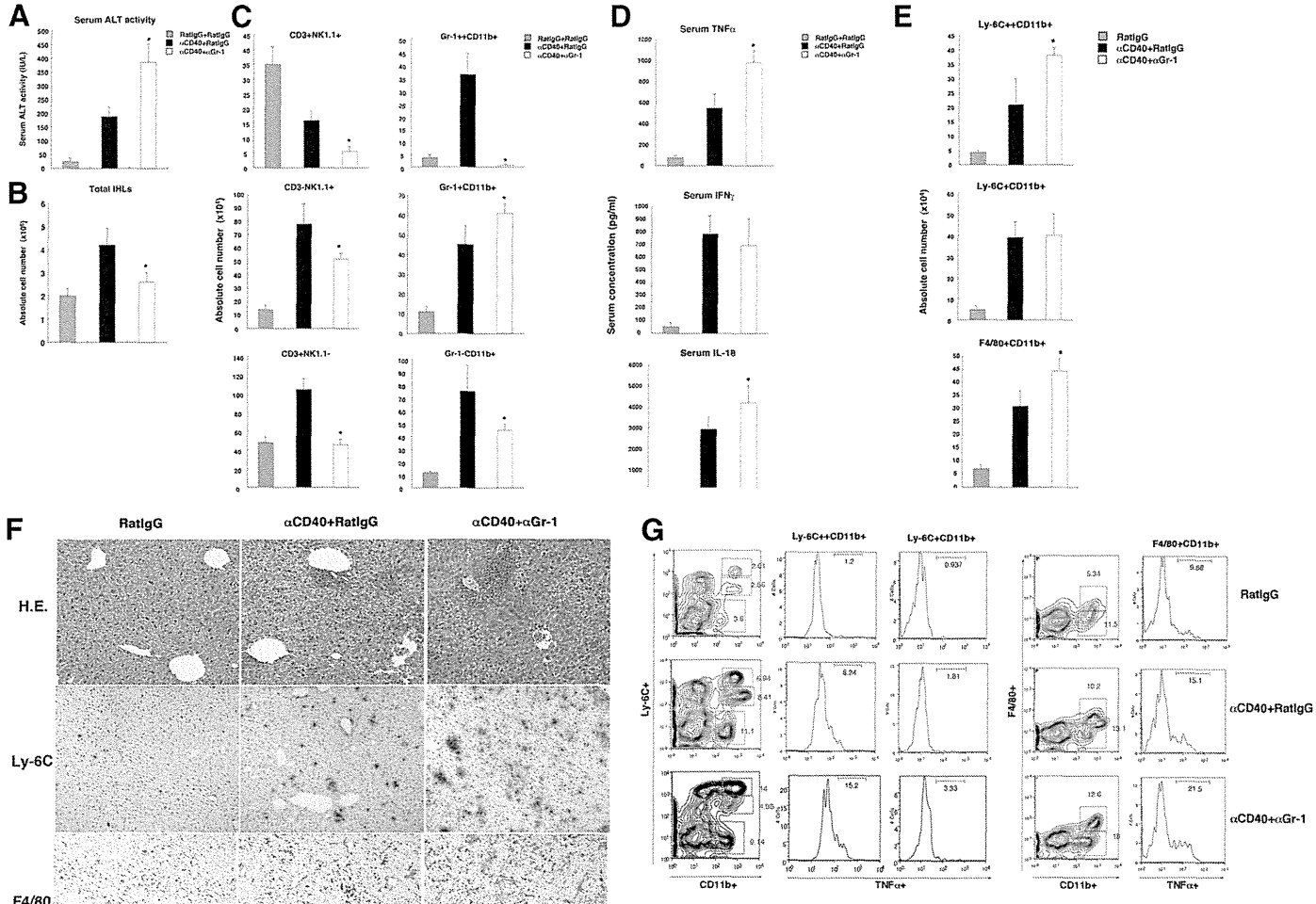

Figure 4. Role of neutrophils. (A) Serum ALT activities. C57BL/6 mice were injected with αCD40 or rat IgG in the absence or presence of αGr-1 mAb and killed after 5 days. Their serum ALT activities were measured and expressed in IU/L; $*P < 0.05$. (B and C) IHLs were isolated from the indicated mice, and the effects of αGr-1 mAb on cell recruitment were analyzed. Data represent the mean + SD; $*P < 0.05$. (D) Serum cytokine concentrations after αCD40 injection in C57BL/6 mice. Data are expressed as the mean + SD; $*P < 0.05$. (E) Numbers of differentiated macrophages. IHLs were stained with anti-CD11b-allophycocyanin, anti-mouse F4/80, and anti-mouse Ly-6C mAb; $*P < 0.05$. (F) Immunohistochemical staining. Liver sections obtained from mice killed at 5 days after injection were stained with H&E or with anti-mouse F4/80, Ly-6C, or Gr-1 mAb. (G) Intracellular cytokine expression levels in macrophages and monocytes. To determine which cell populations produced TNF-α after injection, we stained the cells with anti-mouse F4/80-FITC, Ly-6C-PE, anti-CD11b-allophycocyanin, and anti-TNF-α-PE mAb. The cells were analyzed using a FACSCalibur system.

DISCUSSION

The present study has clarified several important aspects of liver pathology in terms of inflammatory cell recruitment and activation in the liver and provides important findings regarding the interactions among IL-18, macrophages, neutrophils, and NKT cells. The innate immune system, which is considered to provide nonantigen-specific immune responses, can provide emergency signals from destroyed hepatocytes during liver inflammation, resulting in an inflammatory response. These inflammatory events contribute to liver injury and conversely, may also be involved in liver repair based on various experimental liver disease models [18–20]. Therefore, it is well established that an inflammatory response is essential for controlling the microenvironment in the liver, but the relationships among macrophages and other inflammatory cells with regard to liver injury are still obscure. Careful interpretation is required to evaluate the results of the present study, especially with regard to the interactions between IHLs and the liver injury in this model. The liver injury model that we used involves artificial stimulation of macrophages, monocytes, and B cells that express CD40, and these cells subsequently activate NK cells and NKT cells, thereby causing liver injury by way of IFN-γ, TNF-α, and IL-12 [14, 15]. In general, it has

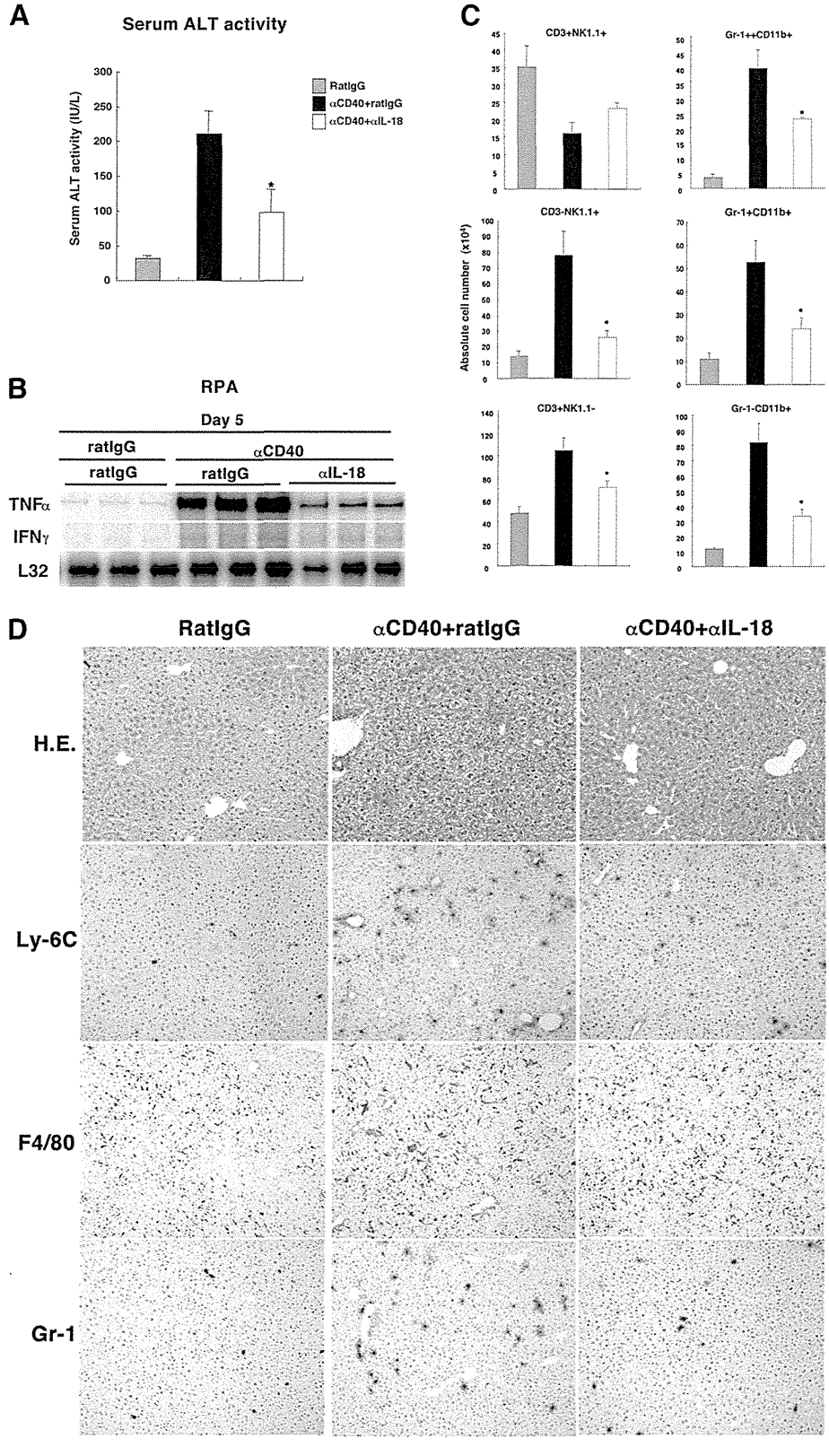

Figure 5. Role of IL-18. (A) Serum ALT activities. C57BL/6 mice were injected with αIL-18 mAb or control rat IgG before injection of αCD40 or rat IgG and killed after 5 days. The serum ALT activities were measured and expressed in IU/L; $*P < 0.05$. (B) Total hepatic RNA was analyzed as described in the legend to Fig. 3. (C) Numbers of differentiated macrophages. IHLs were stained with anti-CD11b-allophycocyanin, anti-mouse F4/80, and anti-mouse Ly-6C mAb; $*P < 0.05$. (D) Immunohistochemical staining. Liver sections obtained from mice killed at 5 days after injection were stained with H&E or with anti-mouse F4/80, Ly-6C, or Gr-1 mAb.

been well understood that the interactions between CD40 and CD40 ligand reciprocally deliver activating signals to APCs and cognate T cells. This process is critically important for the development of adaptive immunity [21–23]. However, we consider that this liver injury model is useful for analyzing how activated macrophages or B cells affect the activation of other IHLs and their recruitment in liver injury, as the agonistic CD40 antibody mainly activates macrophages and B cells.

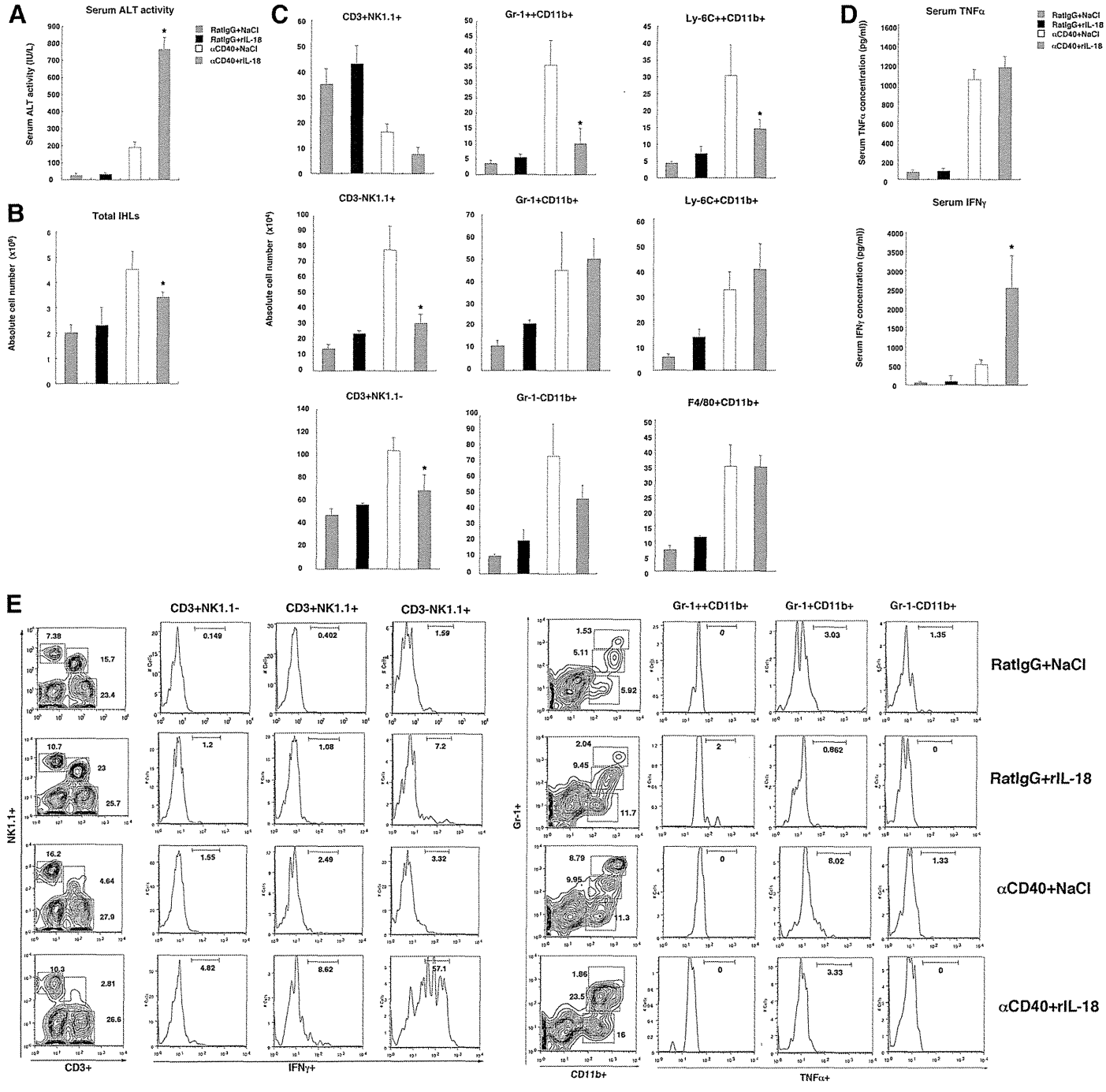

Figure 6. Additional IL-18 treatment exacerbates liver injury after αCD40 injection. (A) Serum ALT activities. C57BL/6 mice were injected with αCD40 or rat IgG in the absence or presence of rIL-18 and killed after 5 days. The serum ALT activities were measured and expressed in IU/L; $^*P < 0.05$. (B and C) IHLs were isolated from the indicated mice, and the effects of IL-18 on cell recruitment were analyzed. Data represent the mean + SD; $^*P < 0.05$. (D) Serum cytokine concentrations after αCD40 injection in C57BL/6 mice. Data are expressed as the mean + SD; $^*P < 0.05$. (E) Intracellular cytokine expression levels in macrophages and monocytes. To determine which cell populations produced TNF-α after injection, we stained the cells with anti-mouse F4/80-FITC, Ly-6C-PE, anti-CD11b-allophycocyanin, and anti-TNF-α-PE mAb. The cells were analyzed using a FACSCalibur system.

First, we determined the characteristics of intrahepatic macrophages, which became activated on Days 1 and 5 after αCD40 injection, as they are key effector cells for the liver injury [14]. We analyzed the proliferation of the macrophages and detected a peak at Day 3. This finding was consistent with the observed numbers of macrophages. Notably, the highly proliferating macrophages were unable to produce TNF-α, and this is considered to be one of the reasons why αCD40-triggered inflammation exhibits a biphasic pattern in the liver. The present study demonstrated that monocyte subsets differing in Ly-6C expression represented different stages in

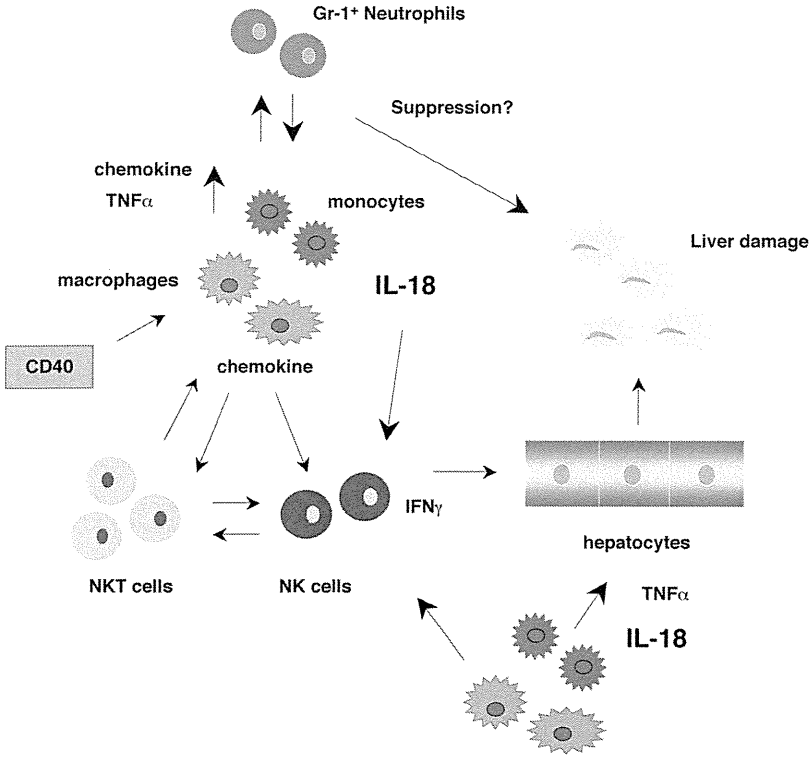

Figure 7. Scheme for how αCD40 triggers liver inflammation. 1) TNF-α and chemokines are produced by activated macrophages after αCD40 stimulation. 2) Neutrophils increase rapidly and control the activation of macrophages or monocytes. 3) At the same time, NKT cells are activated and produce inflammatory cytokines. 4) IL-18 stimulates the migration of macrophages and monocytes into the liver and activates NK cells. 5) Inflammatory cytokines stimulate IFN-γ production by NK cells, and the produced IFN-γ further stimulates macrophages and exacerbates the severe liver injury.

a continuous maturation pathway, and previous in vitro experiments indicated that this transition occurs within 24–48 h [24]. Based on these findings, we suggest that not only the increase in Ly-6C^{high} monocytes, which have suppressive functions [25], but also the high proliferation of macrophages may cause the suppressed inflammatory response at Day 3. Although we investigated the suppressive inflammatory cytokine IL-10, we were unable to confirm the elevated production of this cytokine in the liver at Day 3 compared with Day 5 (Supplemental Fig. 1).

Although tissue macrophages and monocytes increased to reach a peak at Day 3 after injection, neutrophils increased rapidly and were reduced by Day 3. Interestingly, we found that neutrophil depletion exacerbated the αCD40-induced liver injury. In general, neutrophils have an effector function against several liver injury models, such as those involving carbon tetrachloride- and ischemic/perfusion-induced liver injury [26, 27]. These previous studies demonstrated that reactive oxygen from neutrophils is a key factor for hepatocyte damage. Our findings seem to be contradictory to the well-established paradigm that neutrophils induce tissue damage. However, the outcomes of αGr-1 treatment may vary depending on the liver injury models involved, as we have shown already that αGr-1 treatment partially protects against liver injury in hepatitis B virus transgenic mice [28, 29].

A recent report suggested that Gr-1^{high}CD11b^{+} cells suppress T cells in tumor-bearing mice [30] and that Gr-1^{high}CD11b^{low} polymononuclear cell–myeloid-derived suppressor cell populations have suppressive potential in the healthy spleen [31]. These reports suggest the possibility that liver injury is exacerbated by depletion of suppressive, Gr-1-positive cells. Furthermore, we need to confirm whether antibody-tagged neutrophils accumulate in the liver and whether Kupffer cells are activated by phagocytosis. In fact, we found that αGr-1 treatment induced the migration of macrophages and monocytes into the liver, and these cells produced large amounts of TNF-α, indicating that conclusive evidence for whether neutrophils have suppressive effects on this liver injury may require further investigations.

We further found that NKT cells participated in the αCD40-induced biphasic liver injury. NKT cells are particularly abundant in the liver, accounting for 20–30% of IHLs, and are thought to play roles in immunity against intracellular bacteria and parasites and certain tumors [8, 32]. It is well established that CD40 cross-linking induces DCs to up-regulate their expressions of CD40, B7.1, B7.2, and IL-12, which in turn, enhance NKT cell activation and cytokine production [32]. In this liver injury, NKT cells activated other inflammatory cells, including NK cells and macrophages, in the liver, as IFN-γ production by NK cells and TNF-α production by macrophages were apparently blocked in the liver of NKT KO mice. Consistent with the finding that macrophage recruitment was reduced in NKT KO mice, infiltration of the various macrophage subpopulations was also inhibited, indicating that NKT cells have an influence on macrophage differentiation following αCD40 injection. It is of note that NKT cells were secondarily activated by way of CD40 ligation on macrophages and DCs and that NKT KO mice appear to exhibit protection against inflammatory cell recruitment into the liver. These findings demonstrate the importance of NKT cells for the propagation of inflammatory liver disease.

In this study, we have demonstrated that IL-18 is involved in the late-phase liver injury. Although we found that IL-12 played a pivotal role in the early-phase liver injury, IL-18 was not necessary for liver injury to occur, as neutralization of IL-18 did not increase the serum ALT activity (Supplemental Fig. 5). IL-18 is known to induce NK and NKT cells to produce IFN-γ [12], but it

requires IL-12 to induce IFN-γ production by Th1 cells [11]. In keeping with these findings, we found that rIL-18 treatment rapidly induced intrahepatic NK cells to produce large amounts of IFN-γ and also to cause severe liver injury. Importantly, these effects did not involve TNF-α and did not require the recruitment of macrophages, monocytes, and neutrophils into the liver. More recently, intracellular microbial sensors have been identified, including NLRs [33, 34]. Some of the NLRs also sense nonmicrobial danger signals and form large cytoplasmic complexes called inflammasomes, which link the sensing of microbial products and metabolic stress to proteolytic activation of the proinflammatory cytokines IL-1β and IL-18. Therefore, in this model, the danger signals for early liver damage may trigger the activation of inflammasomes, resulting in the production of IL-18 and subsequent induction of liver damage.

In conclusion, the present results demonstrate that activation of intrahepatic macrophages can initiate a cascade of events that begins with the production of inflammatory cytokines and chemokines and leads to the activation of intrahepatic NK and NKT cells for the production of IFN-γ, all of which contribute to the recruitment of additional inflammatory cells to the liver (**Fig. 7**). We have shown that the interactions among macrophages, monocytes, neutrophils, and NKT cells participate efficiently and closely in the exacerbation of liver inflammation through cytokine and chemokine production. Further studies are required to identify the roles of the suppressive monocyte or neutrophil subpopulations in the liver injury, and clarification of the roles of these cell types will be useful in the treatment of various liver diseases.

AUTHORSHIP

K.K. planned the experimental project, and K.K., S.S., S.H., Y.H., T.H., and M.N. performed data analysis and wrote the paper. M.K. contributed data and comments about the manuscript.

ACKNOWLEDGMENTS

This study was supported by a grant-in-aid (B) from the Ministry of Education, Culture, Sports, Science and Technology of Japan (grant no. 20390203) and a grant-in-aid for specially promoted research on viral diseases from the Tokyo Metropolitan Government to K.K. We thank Dr. Francis V. Chisari (The Scripps Research Institute) for supporting this study and Dr. Antonius Rolink (Basel Institute for Immunology) for providing the anti-mouse agonistic CD40 mAb. We are also grateful to Drs. Toshinori Nakayama (Chiba University) and Masaru Taniguchi (RIKEN) for providing the Vα14 NKT KO mice.

REFERENCES

1. Akira, S., Uematsu, S., Takeuchi, O. (2006) Pathogen recognition and innate immunity. *Cell* **124,** 783–801.
2. Crispe, I. N. (2009) The liver as a lymphoid organ. *Annu. Rev. Immunol.* **27,** 147–163.
3. Crispe, I. N. (2003) Hepatic T cells and liver tolerance. *Nat. Rev. Immunol.* **3,** 51–62.
4. Banchereau, J., Briere, F., Caux, C., Davoust, J., Lebecque, S., Liu, Y. J., Pulendran, B., Palucka, K. (2000) Immunobiology of dendritic cells. *Annu. Rev. Immunol.* **18,** 767–811.
5. Munder, M., Mallo, M., Eichmann, K., Modolell, M. (1998) Murine macrophages secrete interferon γ upon combined stimulation with interleukin (IL)-12 and IL-18: a novel pathway of autocrine macrophage activation. *J. Exp. Med.* **187,** 2103–2108.
6. Zlotnik, A., Yoshie, O. (2000) Chemokines: a new classification system and their role in immunity. *Immunity* **12,** 121–127.
7. Wardle, E. N. (1987) Kupffer cells and their function. *Liver* **7,** 63–75.
8. Taniguchi, M., Harada, M., Kojo, S., Nakayama, T., Wakao, H. (2003) The regulatory role of Vα14 NKT cells in innate and acquired immune response. *Annu. Rev. Immunol.* **21,** 483–513.
9. Seino, K., Taniguchi, M. (2005) Functionally distinct NKT cell subsets and subtypes. *J. Exp. Med.* **202,** 1623–1626.
10. Van Kaer, L., Joyce, S. (2005) Innate immunity: NKT cells in the spotlight. *Curr. Biol.* **15,** R429–R431.
11. Nakanishi, K., Yoshimoto, T., Tsutsui, H., Okamura, H. (2001) Interleukin-18 regulates both Th1 and Th2 responses. *Annu. Rev. Immunol.* **19,** 423–474.
12. Okamura, H., Kashiwamura, S., Tsutsui, H., Yoshimoto, T., Nakanishi, K. (1998) Regulation of interferon-γ production by IL-12 and IL-18. *Curr. Opin. Immunol.* **10,** 259–264.
13. Kimura, K., Kakimi, K., Wieland, S., Guidotti, L. G., Chisari, F. V. (2002) Interleukin-18 inhibits hepatitis B virus replication in the livers of transgenic mice. *J. Virol.* **76,** 10702–10707.
14. Kimura, K., Kakimi, K., Wieland, S., Guidotti, L. G., Chisari, F. V. (2002) Activated intrahepatic antigen-presenting cells inhibit hepatitis B virus replication in the liver of transgenic mice. *J. Immunol.* **169,** 5188–5195.
15. Kimura, K., Moriwaki, H., Nagaki, M., Saio, M., Nakamoto, Y., Naito, M., Kuwata, K., Chisari, F. V. (2006) Pathogenic role of B cells in anti-CD40-induced necroinflammatory liver disease. *Am. J. Pathol.* **168,** 786–795.
16. Rolink, A., Melchers, F., Andersson, J. (1996) The SCID but not the RAG-2 gene product is required for S μ-S ε heavy chain class switching. *Immunity* **5,** 319–330.
17. Naito, M., Nagai, H., Kawano, S., Umezu, H., Zhu, H., Moriyama, H., Yamamoto, T., Takatsuka, H., Takei, Y. (1996) Liposome-encapsulated dichloromethylene diphosphonate induces macrophage apoptosis in vivo and in vitro. *J. Leukoc. Biol.* **60,** 337–344.
18. Gao, B., Jeong, W. I., Tian, Z. (2008) Liver: an organ with predominant innate immunity. *Hepatology* **47,** 729–736.
19. Guidotti, L. G., Chisari, F. V. (2001) Noncytolytic control of viral infections by the innate and adaptive immune response. *Annu. Rev. Immunol.* **19,** 65–91.
20. Jaeschke, H., Bajt, M. L. (2004) Critical role of CXC chemokines in endotoxemic liver injury in mice. *J. Leukoc. Biol.* **76,** 1089–1090, author reply 1091–1092.
21. Banchereau, J., Bazan, F., Blanchard, D., Briere, F., Galizzi, J. P., van Kooten, C., Liu, Y. J., Rousset, F., Saeland, S. (1994) The CD40 antigen and its ligand. *Annu. Rev. Immunol.* **12,** 881–922.
22. Cella, M., Scheidegger, D., Palmer-Lehmann, K., Lane, P., Lanzavecchia, A., Alber, G. (1996) Ligation of CD40 on dendritic cells triggers production of high levels of interleukin-12 and enhances T cell stimulatory capacity: T-T help via APC activation. *J. Exp. Med.* **184,** 747–752.
23. Grewal, I. S., Flavell, R. A. (1998) CD40 and CD154 in cell-mediated immunity. *Annu. Rev. Immunol.* **16,** 111–135.
24. Leenen, P. J., de Bruijn, M. F., Voerman, J. S., Campbell, P. A., van Ewijk, W. (1994) Markers of mouse macrophage development detected by monoclonal antibodies. *J. Immunol. Methods* **174,** 5–19.
25. Zhu, B., Bando, Y., Xiao, S., Yang, K., Anderson, A. C., Kuchroo, V. K., Khoury, S. J. (2007) CD11b+Ly-6C(hi) suppressive monocytes in experimental autoimmune encephalomyelitis. *J. Immunol.* **179,** 5228–5237.
26. Duffield, J. S., Forbes, S. J., Constandinou, C. M., Clay, S., Partolina, M., Vuthoori, S., Wu, S., Lang, R., Iredale, J. P. (2005) Selective depletion of macrophages reveals distinct, opposing roles during liver injury and repair. *J. Clin. Invest.* **115,** 56–65.
27. Luster, M. I., Simeonova, P. P., Gallucci, R. M., Bruccoleri, A., Blazka, M. E., Yucesoy, B. (2001) Role of inflammation in chemical-induced hepatotoxicity. *Toxicol. Lett.* **120,** 317–321.
28. Takai, S., Kimura, K., Nagaki, M., Satake, S., Kakimi, K., Moriwaki, H. (2005) Blockade of neutrophil elastase attenuates severe liver injury in hepatitis B transgenic mice. *J. Virol.* **79,** 15142–15150.
29. Sitia, G., Isogawa, M., Kakimi, K., Wieland, S. F., Chisari, F. V., Guidotti, L. G. (2002) Depletion of neutrophils blocks the recruitment of antigen-nonspecific cells into the liver without affecting the antiviral activity of hepatitis B virus-specific cytotoxic T lymphocytes. *Proc. Natl. Acad. Sci. USA* **99,** 13717–13722.
30. Dolcetti, L., Peranzoni, E., Ugel, S., Marigo, I., Fernandez Gomez, A., Mesa, C., Geilich, M., Winkels, G., Traggiai, E., Casati, A., Grassi, F., Bronte, V. (2010) Hierarchy of immunosuppressive strength among myeloid-derived suppressor cell subsets is determined by GM-CSF. *Eur. J. Immunol.* **40,** 22–35.
31. Greifenberg, V., Ribechini, E., Rossner, S., Lutz, M. B. (2009) Myeloid-derived suppressor cell activation by combined LPS and IFN-γ treatment impairs DC development. *Eur. J. Immunol.* **39,** 2865–2876.
32. Kronenberg, M. (2005) Toward an understanding of NKT cell biology: progress and paradoxes. *Annu. Rev. Immunol.* **23,** 877–900.
33. Martinon, F., Mayor, A., Tschopp, J. (2009) The inflammasomes: guardians of the body. *Annu. Rev. Immunol.* **27,** 229–265.
34. Pétrilli, V., Dostert, C., Muruve, D. A., Tschopp, J. (2007) The inflammasome: a danger sensing complex triggering innate immunity. *Curr. Opin. Immunol.* **19,** 615–622.

KEY WORDS:
neutrophil · macrophage · NKT cell · chemokine · IL-18

Incorporation of Biaryl Units into the 5′ and 3′ Ends of Sense and Antisense Strands of siRNA Duplexes Improves Strand Selectivity and Nuclease Resistance

Kayo Yoshikawa,[†] Aya Ogata,[†] Chiho Matsuda,[§] Michinori Kohara,[§] Hideo Iba,[||] Yukio Kitade,[†,‡] and Yoshihito Ueno*,[†,‡]

Department of Biomolecular Science, Faculty of Engineering, and United Graduate School of Drug Discovery and Medical Information Sciences, Gifu University, 1-1 Yanagido, Gifu 501-1193, Japan, Department of Microbiology and Cell Biology, The Tokyo Metropolitan Institute of Medical Science, 2-1-6, Kamikitazawa, Setagaya-ku, Tokyo 156-0057, Japan, and Division of Host-Parasite Interaction, Department of Microbiology and Immunology, Institute of Medical Science, The University of Tokyo, 4-6-1 Shirokanedai, Minato-ku, Tokyo 108-8639, Japan. Received July 5, 2010; Revised Manuscript Received November 30, 2010

Small interfering RNA (siRNA) is a noncoding RNA with considerable potential as a new therapeutic drug for intractable diseases. siRNAs can be rationally designed and synthesized if the sequences of the disease-causing genes are known. In this paper, we describe the synthesis and properties of siRNAs modified with biaryl units. We found that incorporation of biaryl units into the 5′ and 3′ ends of sense and antisense strands of siRNA duplexes improved strand selectivity and nuclease resistance.

INTRODUCTION

RNA interference (RNAi) is a biological process whereby double-stranded RNAs (dsRNAs) silence gene expression in a sequence-specific manner (*1*). Small RNAs, including small interfering RNA (siRNA) and microRNA (miRNA), are key intermediates in RNAi. They regulate gene expression through the RNA-induced silencing complex (RISC), which contains Argonaute proteins as core components. siRNAs hold considerable potential as new therapeutic drugs for intractable diseases, because they can be rationally designed and synthesized if the sequences of disease-causing genes are known (*2*–*6*).

One strand from an siRNA or miRNA duplex is selected and loaded onto RISC to become mature siRNA or miRNA. It has been suggested that RISC preferentially selects and incorporates one of two strands of the siRNA duplex, depending on its thermodynamic features. The strand with thermodynamically lower stability in its 5′-terminus (the guide strand) preferentially binds the RISC and becomes functional, whereas the other strand (the passenger strand) is degraded (*7*–*9*). However, it has recently become clear that strand selection does not always follow this rule (*1*–*14*). Recently reported siRNA studies demonstrated that modifying the 5′-terminus of one strand with 5′-*O*-methyl efficiently specifies its antisense strand to be loaded onto RISC despite thermodynamic disadvantages (*15*), because 5′-*O*-methyl inhibits phosphorylation of the 5′-terminus, which is an important factor for RISC loading (*16*–*20*).

We have reported the synthesis of DNAs containing biaryl units, **3** and **5**, which comprised benzene and naphthalene or pyrene residues (Figure 1). The biaryl units thermally and thermodynamically stabilized DNA/DNA duplexes (*21*). We have also succeeded in improving siRNA nuclease resistance by introduction of bis(hydroxymethyl)benzene (**1**) instead of thymidine at 3′-overhangs without reducing RNAi-inducing activity (*22*). From these results and background information, we planned the synthesis of siRNAs with biaryl units at the 5′ and 3′ ends of sense and antisense strands of siRNA duplexes, respectively. We expected that thermal and thermodynamic stabilities of the 5′ regions of siRNA sense strands would be increased by these biaryl modifications. Phosphorylation of the 5′ ends of sense strands, an important factor for RISC loading, was expected to be inhibited by biaryl protection of 5′-hydroxyls. We anticipated that these modifications would enhance RISC loading of antisense strands of siRNA duplexes, suppressing off-target effects induced by sense strands. We also anticipated improved nuclease resistance in biaryl-modified siRNAs, which is important for the therapeutic application of synthetic siRNAs.

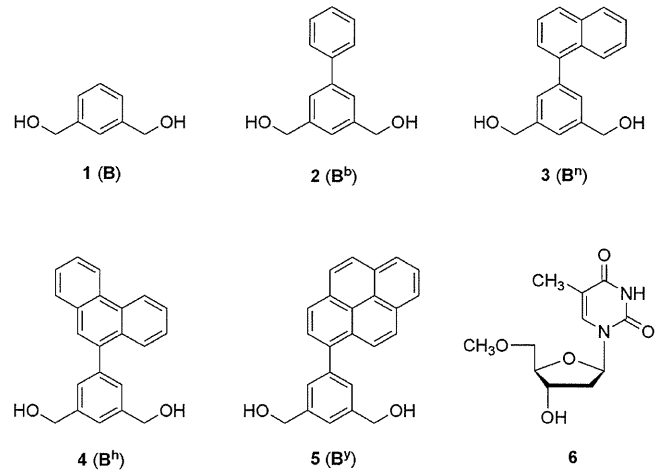

Figure 1. Structures of the aromatic compounds and modified nucleoside used in this study.

In this paper, we report the synthesis and properties of siRNA duplexes which carry biaryl units at the 5′ and 3′ ends of sense and antisense strands, respectively. We assessed the gene

* To whom correspondence should be addressed. Phone: +81-58-293-2639. Fax: +81-58-293-2794. E-mail: uenoy@gifu-u.ac.jp.
† Department of Biomolecular Science, Faculty of Engineering, Gifu University.
‡ United Graduate School of Drug Discovery and Medical Information Sciences, Gifu University.
§ The Tokyo Metropolitan Institute of Medical Science.
|| The University of Tokyo.

10.1021/bc100301w
Published on Web 12/09/2010

Scheme 1[a]

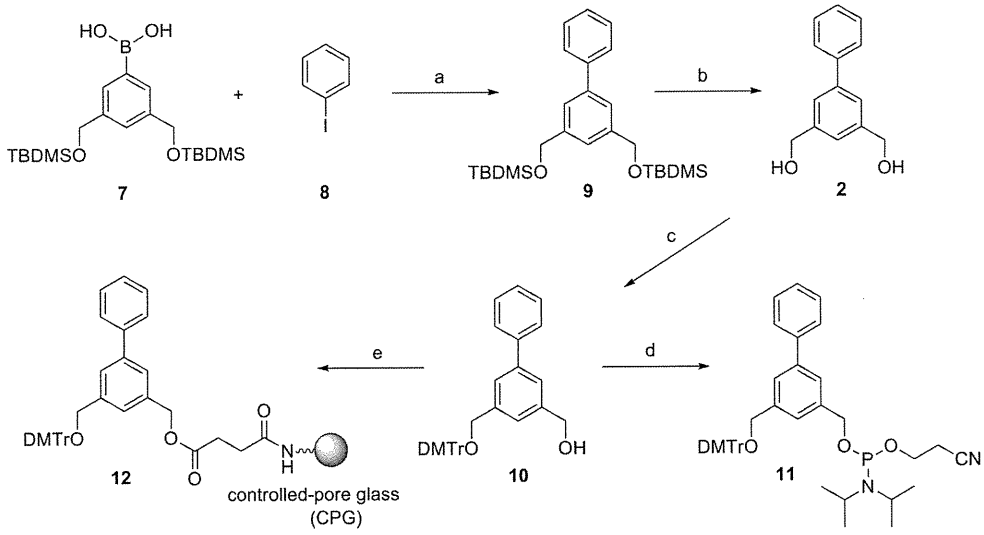

[a] Reagents and conditions: (a) $PdCl_2(dppf)\cdot CH_2Cl_2$, NaOH, THF/$H_2O$ (5:1 v/v), 65 °C, 24 h; (b) TBAF, THF, rt, 2 h, 93% from **7**; (c) DMTrCl, pyridine, rt, 4 h, 52%; (d) chloro(2-cyanoethoxy)(*N*,*N*-diisopropylamino)phosphane, *i*-Pr_2NEt, THF, rt, 1 h, 88%; (e) (1) succinic anhydride, DMAP, pyridine, rt, 24 h; (2) CPG, EDCI, DMF, rt, 48 h, 49 μmol/g loading amount.

Scheme 2[a]

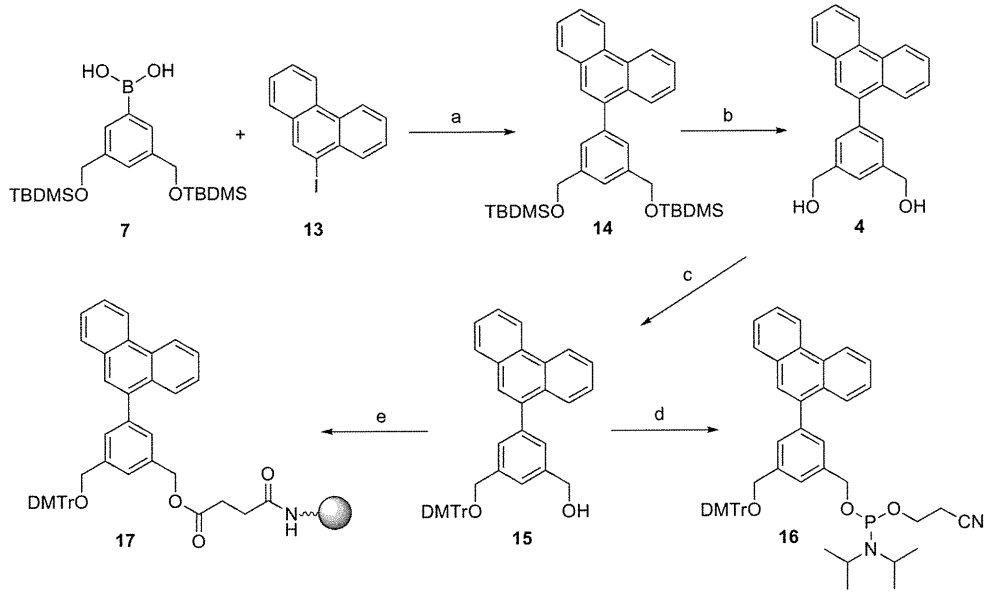

[a] Reagents and conditions: (a) $PdCl_2(dppf)\cdot CH_2Cl_2$, NaOH, THF/$H_2O$ (5:1 v/v), 65 °C, 24 h; (b) TBAF, THF, rt, 2 h, 60% from **7**; (c) DMTrCl, pyridine, rt, 3 h, 61%; (d) chloro(2-cyanoethoxy)(*N*,*N*-diisopropylamino)phosphane, *i*-Pr_2NEt, THF, rt, 1 h, 74%; (e) (1) succinic anhydride, DMAP, pyridine, rt, 24 h; (2) CPG, EDCI, DMF, rt, 48 h, 45 μmol/g loading amount.

silencing activities of the modified siRNAs by a dual-luciferase assay. We also assessed the nuclease-resistance of the modified siRNAs.

RESULTS AND DISCUSSION

Design and Synthesis of siRNAs. The Argonaute proteins are core components of RISC, which is responsible for mRNA cleavage in the RNAi pathway. The proteins are composed of PAZ, Mid, and PIWI domains. X-ray structural analysis and a nuclear magnetic resonance (NMR) study have revealed that the 3′-overhang region of a guide strand of siRNA is recognized by the PAZ domain and the 2-nucleotide (nt) 3′-overhang is accommodated by a binding pocket composed of hydrophobic amino acids (*23*−*26*). In order to estimate the appropriate size for biaryl units in the 3′-overhang region, we assessed the silencing activities of siRNAs which carried various types of biaryl units at the 3′-overhangs.

We assessed the biaryl units **2** ($\mathbf{B^b}$), **3** ($\mathbf{B^n}$), **4** ($\mathbf{B^h}$), and **5** ($\mathbf{B^y}$), comprising benzene and benzene, naphthalene, phenanthrene, or pyrene residues, to determine the appropriate size for the 3′-overhang regions. Phosphoramidites of **3** and **5** were synthesized according to a previously reported method (*21*). Phosphoramidites of **2** and **4** and solid supports carrying **2** or **4** were synthesized according to the methods shown in Schemes 1 and 2. An arylboronic acid derivative **7** was coupled with iodobenzene (**8**) in the presence of $PdCl_2(dppf)$ (dppf stands for 1,1′-bis(diphenylphosphanyl)ferrocene) at 65 °C; this coupling reaction produced the biaryl derivative **9**; subsequently, **9** was desilylated by treatment with tetra-*n*-butylammonium fluoride (TBAF) to give a 93% yield of biaryl unit **2.** One out of the two hydroxy groups of **2** was protected by a 4,4′-dimethoxytrityl (DMTr) group to give a 52% yield of mono-DMTr derivative **10**. **10** was phosphitylated by the standard procedure to produce the corresponding phosphoramidite **11** at

Table 1. Sequences of ONs and siRNAs[a]

no. of siRNA	no. of ON	sequence
siRNA**18**	ON**43**	5′-GGCCUUUCACUACUCCUAC*tt*-3′
	ON**44**	3′-*tt*CCGGAAAGUGAUGAGGAUG-5′
siRNA**19**	ON**45**	5′-GGCCUUUCACUACUCCUAC**B^{b}B^b**-3′
	ON**46**	3′-**B^{b}B^b**CCGGAAAGUGAUGAGGAUG-5′
siRNA**20**	ON**47**	5′-GGCCUUUCACUACUCCUAC**B^{n}B^n**-3′
	ON**48**	3′-**B^{n}B^n**CCGGAAAGUGAUGAGGAUG-5′
siRNA**21**	ON**49**	5′-GGCCUUUCACUACUCCUAC**B^{h}B^h**-3′
	ON**50**	3′-**B^{h}B^h**CCGGAAAGUGAUGAGGAUG-5′
siRNA**22**	ON**51**	5′-GGCCUUUCACUACUCCUAC**B^{y}B^y**-3′
	ON**52**	3′-**B^{y}B^y**CCGGAAAGUGAUGAGGAUG-5′
siRNA**23**	ON**53**	**F**-5′-GGCCUUUCACUACUCCUAC*tt*-3′
	ON**44**	3′-*tt*CCGGAAAGUGAUGAGGAUG-5′
siRNA**24**	ON**54**	**F**-5′-GGCCUUUCACUACUCCUAC**B^{b}B^b**-3′
	ON**46**	3′-**B^{b}B^b**CCGGAAAGUGAUGAGGAUG-5′
siRNA**25**	ON**55**	5′-CUUCUUCGUCGAGACCAUG*tt*-3′
	ON**56**	3′-*tt*GAAGAAGCAGCUCUGGUAC-5′
siRNA**26**	ON**57**	5′-**B^b**CUUCUUCGUCGAGACCAUG*tt*-3′
	ON**56**	3′-*tt*GAAGAAGCAGCUCUGGUAC-5′
siRNA**27**	ON**58**	5′-**B^n**CUUCUUCGUCGAGACCAUG*tt*-3′
	ON**56**	3′-*tt*GAAGAAGCAGCUCUGGUAC-5′
siRNA**28**	ON**55**	5′-CUUCUUCGUCGAGACCAUG*tt*-3′
	ON**59**	3′-*tt*GAAGAAGCAGCUCUGGUAC**B^b**-5′
siRNA**29**	ON**55**	5′-CUUCUUCGUCGAGACCAUG*tt*-3′
	ON**60**	3′-*tt*GAAGAAGCAGCUCUGGUAC**B^n**-5′
siRNA**30**	ON**61**	5′-UUUCACUACUCCUACGAGC*tt*-3′
	ON**62**	3′-*tt*AAAGUGAUGAGGAUGCUCG-5′
siRNA**31**	ON**63**	5′-**B^n**UUUCACUACUCCUACGAGC**BB**-3′
	ON**64**	3′-**BB^n**AAAGUGAUGAGGAUGCUCG-5′
siRNA**32**	ON**63**	5′-**B^n**UUUCACUACUCCUACGAGC**BB**-3′
	ON**65**	3′-**B^{n}B^n**AAAGUGAUGAGGAUGCUCG-5′
siRNA**33**	ON**66**	5′-**T^m**UUCACUACUCCUACGAGC*tt*-3′
	ON**62**	3′-*tt*AAAGUGAUGAGGAUGCUCG-5′
siRNA**34**	ON**67**	5′-UAAGAUGUUCAUCGAGUCC*tt*-3′
	ON**68**	3′-*tt*AUUCUACAAGUAGCUCAGG-5′
siRNA**35**	ON**69**	5′-**B^n**UAAGAUGUUCAUCGAGUCC**BB**-3′
	ON**70**	3′-**BB^n**AUUCUACAAGUAGCUCAGG-5′
siRNA**36**	ON**69**	5′-**B^n**UAAGAUGUUCAUCGAGUCC**BB**-3′
	ON**71**	3′-**B^{n}B^n**AUUCUACAAGUAGCUCAGG-5′
siRNA**37**	ON**72**	5′-GUCUCGUAGACCGUGCAUCA*tt*-3′
	ON**73**	3′-*tt*CAGAGCAUCUGGCACGUAGU-5′
siRNA**38**	ON**74**	5′-GUCUCGUAGACCGUGCAUCA**BB**-3′
	ON**75**	3′-**BB**CAGAGCAUCUGGCACGUAGU-5′
siRNA**39**	ON**76**	5′-**B^n**GUCUCGUAGACCGUGCAUCA**BB**-3′
	ON**77**	3′-**BB^n**CAGAGCAUCUGGCACGUAGU-5′
siRNA**40**	ON**76**	5′-**B^n**GUCUCGUAGACCGUGCAUCA**BB**-3′
	ON**75**	3′-**BB**CAGAGCAUCUGGCACGUAGU-5′
siRNA**41**	ON**74**	5′-GUCUCGUAGACCGUGCAUCA**BB**-3′
	ON**77**	3′-**BB^n**CAGAGCAUCUGGCACGUAGU-5′
siRNA**42**	ON**78**	5′-**B^n**GUCUCAUAGGCCAUGCGUCA**BB**-3′
	ON**79**	3′-**BB^n**CAGAGUAUCCGGUACGCAGU-5′

[a] The small italic letters represent 2′-deoxyribonucleosides. The underlined letters indicate mismatched bases. **F** shows fluorescein.

an 88% yield. In a similar manner, phosphoramidite **16** was synthesized from 9-iodophenanthrene (**13**); the total yield of **16** was 27%.

To enable attachment to the solid support, the mono-DMTr derivative **10** was succinated to yield the corresponding succinate, which was linked to controlled pore glass (CPG) to create the solid support **12** linked to **10** (49 μmol/g). Similarly, the mono-DMTr derivative **15** was succinated and linked to the CPGs to yield the solid supports **17** linked to **15** (45 μmol/g). siRNA sequences used in this study are depicted in Table 1.

Thermal Denaturation Study of siRNAs. Thermal stability of biaryl-modified siRNAs was studied by thermal denaturation in 0.01 M sodium phosphate buffer (pH 7.0) containing 0.1 M NaCl (Table 2). The melting temperature (T_ms) of unmodified siRNA**18** was 79.1 °C, while those of siRNAs **19**, **20**, **21**, and **22** were 77.9, 80.7, 82.2, and 82.8 °C, respectively. The siRNA duplexes were found to become more thermostable with increasing biaryl unit size. This result suggests that thermal stabilization of the duplexes is attributable to stacking interactions of the biaryl units with adjacent nucleotides.

Table 2. T_m Values[a]

no. of siRNA	T_m (°C)	ΔT_m (°C)
siRNA**18**	79.1	-
siRNA**19**	79.9	+0.8
siRNA**20**	80.7	+1.6
siRNA**21**	82.2	+3.1
siRNA**22**	82.8	+3.7

[a] The experimental conditions are as described in the Experimental Section.

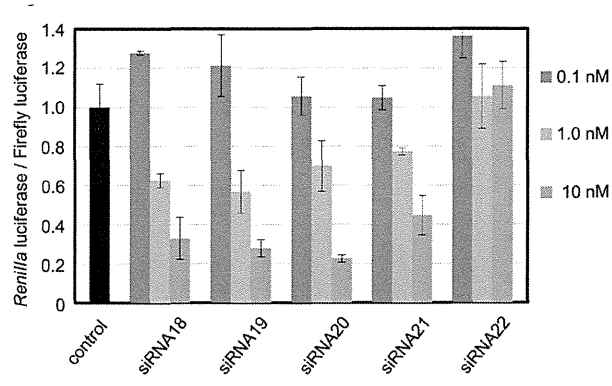

Figure 2. Dual-luciferase assay (1). The experimental conditions are as described in the Experimental Section.

Dual-Luciferase Assay. We assessed the silencing activity of modified siRNAs by performing a dual-luciferase assay using the psiCHECK-2 vector. siRNA sequences were designed to target *Renilla* luciferase. Reporter vectors and synthesized siRNA duplexes were cotransfected into HeLa cells, and luciferase activities were measured after 24 h. The signals of *Renilla* luciferase were normalized to those of firefly luciferase.

As shown in Figure 2, siRNA**18**, **19**, and **20**, which carried natural thymidines, **B^b**s or **B^n**s at their 3′-overhangs, effectively reduced luciferase activity in a dose-dependent manner. In contrast, the silencing activity of siRNA**21**, which contained **B^h** comprising a tricyclic phenanthrene residue, was apparently weaker than that of unmodified siRNA**18**. Further, siRNA**22**, which carried **B^y** with a tetracyclic pyrene residue, had no silencing activity. Thus, biaryl units smaller than the naphthalene type are acceptable for the 3′-overhang region of siRNAs. These results are consistent with a recent report from Somoza et al (*27*).

Microarray profiling studies have demonstrated that siRNAs may silence multiple genes in addition to the intended target (*28, 29*). This unintended (off-target) transcript silencing is a critical problem associated with RNAi-based therapeutic applications. Both the sense and antisense strands of an siRNA can contribute to the off-target effects. Thus, to minimize the extent of sense-strand incorporation into an activated RISC, we next examined the silencing activity of siRNAs, which involved the biaryl units at the 5′ ends of sense or antisense strands of siRNA duplexes. We expected that inhibition of 5′-*O*-phosphorylation of sense strands with biaryl protection of 5′-hydroxyls would enhance RISC loading of antisense strands.

Figure 3a shows the results of siRNAs modified at the 5′ ends of sense strands with biaryl units **B^b** and **B^n**, whereas Figure 3b represents those modified at the 5′ ends of antisense strands. Modifications at the 5′ ends of sense strands did not influence siRNA silencing activity, whereas modifications at the 5′ ends of antisense strands markedly reduced silencing activity. Thus, it was found that the biaryl modifications at the 5′-termini of the sense strands could induce the antisense strand specificity of the siRNA duplexes.

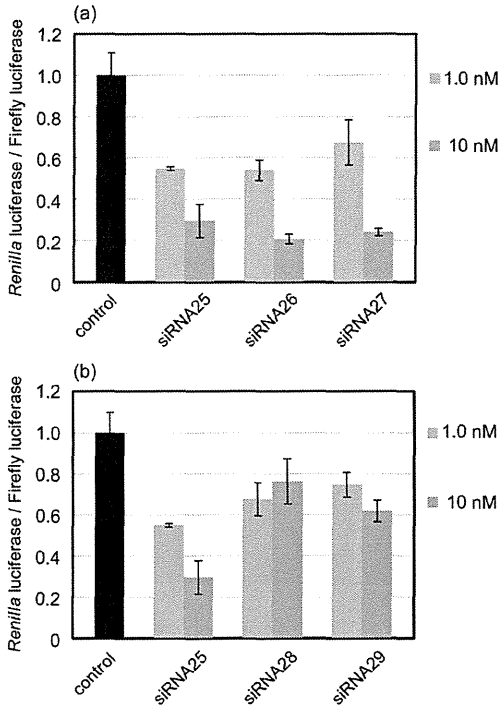

Figure 3. Dual-luciferase assay (2). (a) siRNAs modified at 5′-ends of passenger (sense) strands. (b) siRNAs modified at 5′-ends of guide (antisense) strands.

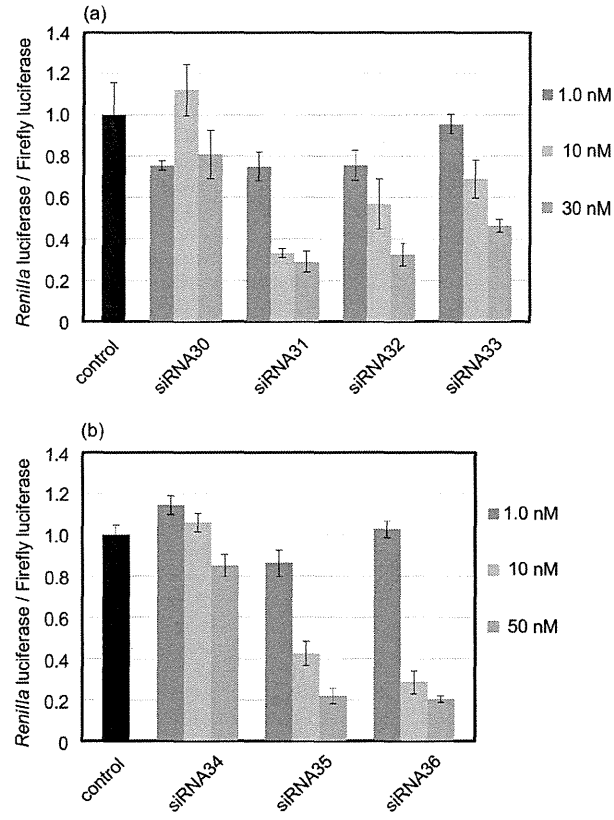

Figure 4. Dual-luciferase assay (3). The experimental conditions are as given in the Experimental Section.

Next, we designed siRNAs which carried biaryl units at the 5′ and 3′ ends of sense and antisense strands, respectively. We speculated that incorporation of the biaryl units into the 5′ and 3′ ends of sense and antisense strands of siRNAs would increase the thermal and thermodynamic stabilities of the sense-strand 5′ siRNA regions. Further, introduction of the biaryl units at the 5′ ends of sense strands would inhibit phosphorylation, which is an important factor for RISC loading. We hypothesized that these modifications would work synergistically, creating more potent siRNAs.

We selected target sequences containing high frequencies of U and A bases, which are thought to be unsuitable targets for siRNA (Table 1). The results of dual-luciferase assays are shown in Figure 4a and b. Unmodified siRNA**30** exhibited almost no silencing activity, whereas siRNA**31** and **32** modified with **B** and **B**^{n} reduced luciferase activity in a dose-dependent manner (Figure 4a). Silencing activities of biaryl-modified siRNA**31** and **32** were greater than that of siRNA**33** containing 5′-*O*-methylthymidine at the 5′ end of the sense strand at all concentrations. This indicates that not only inhibition of phosphorylation, but also thermal stabilization of the 5′ regions of sense strands, contributes to improving siRNA silencing activity. Similarly, unmodified siRNA**34** had almost no silencing activity, whereas biaryl-modified siRNA**35** and **36** efficiently suppressed luciferase expression in a dose-dependent manner (Figure 4b). These results suggest that biaryl modification may provide a good method for improving siRNA silencing activities of sequences which are thought to be unsuitable siRNA targets.

Nuclease Resistance. Improving the nuclease resistance of siRNA is important for the therapeutic application of synthetic siRNAs. It was expected that biaryl-modified RNAs would be more nuclease resistant than unmodified RNAs. First, the susceptibility of the ONs to snake venom phosphodiesterase (SVPD), a 3′-exonuclease, was examined. Unmodified ON**53** and modified ON**54**, which were labeled at the 5′-ends with fluorescein, were incubated with SVPD. The reactions were analyzed using PAGE under denaturing conditions. As shown in Figure 5a, unmodified ON**53** was hydrolyzed randomly after

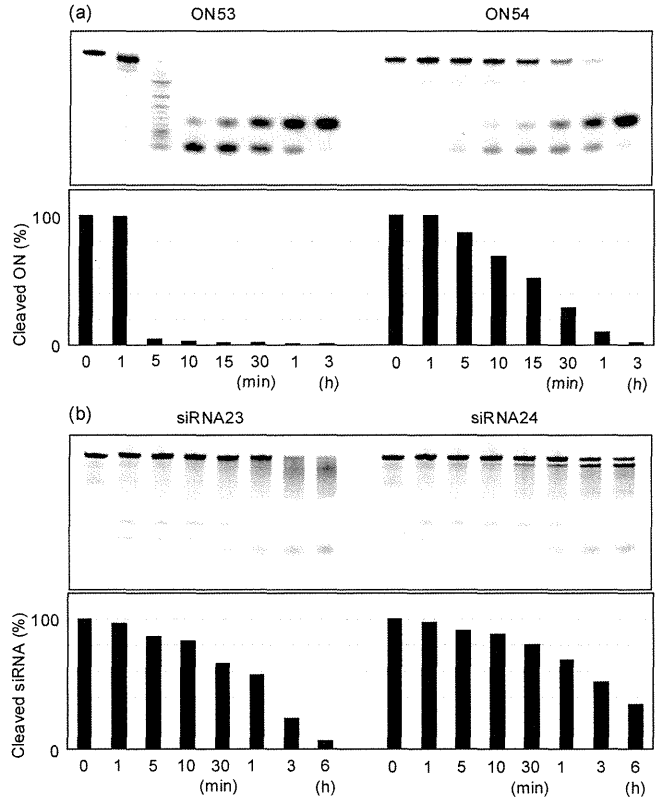

Figure 5. (a) 20% PAGE of 5′-fluorescein-labeled ONs hydrolyzed by SVPD. (b) 20% PAGE of 5′-fluorescein-labeled siRNAs incubated in PBS containing 40% bovine serum. The experimental conditions are as described in the Experimental Section.

5 min of incubation, while modified ON**54** was resistant to the enzyme. The half-life ($t_{1/2}$) of unmodified ON**53** was less than

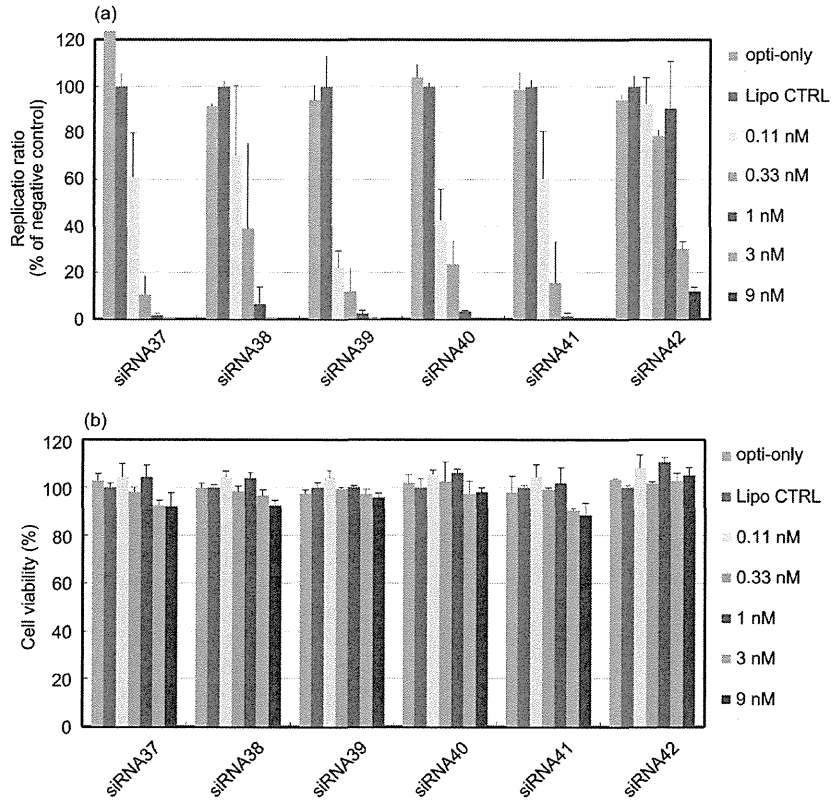

Figure 6. Effect of siRNAs on HCV replication. (a) Inhibition of HCV replication by siRNAs in R6FLR-N replicon cells. HCV replication was calculated by measuring the luminescence ratio with a Bright-Glo luciferase assay system. (b) Cell viability was determined by a WST-8 assay. Data are represented as mean (SD) (n = 3). The experimental conditions are as described in the Experimental Section.

5 min, whereas that of the modified ON**54** was 17 min. ON**54** carrying $\mathbf{B}^{\mathbf{b}}$ at its 3′-end was significantly more resistant to SVPD than unmodified ON**53**.

Next, the stability of siRNAs in PBS containing bovine serum was investigated. Unmodified siRNA**23** and modified siRNA**24**, which were fluorescein-labeled at the 5′ ends of sense strands, were incubated in PBS containing 40% bovine serum. The reactions were analyzed with PAGE under nondenaturing conditions. Figure 5b shows the results. After 6 h of incubation, the band corresponding to the modified siRNA**24** duplex was observed, while that corresponding to the unmodified siRNA**23** duplex was not observed. Thus, the biaryl-modified siRNA**24** is more stable in PBS containing bovine serum than the unmodified siRNA**23**.

Inhibition of HCV Replication. The genome of hepatitis C virus (HCV) is encoded in an approximately 9.6 kb single-stranded RNA. Previously, we have shown that HCV replication is efficiently suppressed by siRNA**38** carrying a benzenephosphate backbone at its 3′-overhang region (*22*). To assess the efficacy of biaryl-modified siRNAs, we compared the HCV replication-suppressing abilities of modified siRNAs with those of unmodified siRNAs. HCV replication is efficiently suppressed by siRNA targeted to an internal ribosome entry site (IRES) region (*30*), which was chosen as the target for this study. siRNA**38**, **39**, **40**, and **41** contain **B** or $\mathbf{B}^{\mathbf{n}}$ at the 5′ or 3′ ends of sense and antisense strands. siRNA**42** carries 4 mismatched bases in its sequence.

Figure 6 shows the results. The modified siRNAs, **38**−**41**, exhibited dose-dependent inhibition of HCV replication. They almost completely suppressed HCV replication at a concentration of 1 nM, while the replication ratio of siRNA**42**, which contained the mismatched bases, was 75% at the same concentration (Figure 6a). The siRNAs exerted no cytotoxic effect at 9 nM (Figure 6b). Thus, it was found that the modified siRNAs **38**−**41** suppressed HCV replication in a sequence-specific manner. At 0.11 nM, siRNA**39**, which carries the naphthalene type of biaryl unit, $\mathbf{B}^{\mathbf{n}}$, at the 5′ and 3′ ends of sense and antisense strands, was the most potent. Thus, $\mathbf{B}^{\mathbf{n}}$ modification also effectively improves the silencing activity of siRNAs targeting HCV.

In conclusion, we have demonstrated the synthesis of siRNAs modified with biaryl units. It was found that incorporation of the naphthalene biaryl unit, $\mathbf{B}^{\mathbf{n}}$, at the 5′ and 3′ ends of sense and antisense strands of siRNA improves silencing activity and nuclease resistance. Further, it was revealed that the modified siRNA suppressed HCV replication more efficiently than unmodified siRNA. Thus, the $\mathbf{B}^{\mathbf{n}}$ modification may hold promise as a method for improvement of the silencing activity and nuclease-resistance of siRNAs. Recently, it has been reported that lipophilic conjugates of oligonucleotides stimulate nonspecific immune response (*31*). The effects of the biaryl modifications of siRNAs on immune response are now under investigation.

EXPERIMENTAL SECTION

General Remarks. The NMR spectra were recorded at 400 MHz (^{1}H) and 100 MHz (^{13}C) and were reported in ppm downfield from tetramethylsilane. The coupling constants (J) are expressed in Hertz. Thin-layer chromatography was carried out on Merck coated plates $60F_{254}$. Silica gel column chromatography was carried out on Wakogel C-300.

1-[3,5-Bis(hydroxymethyl)phenyl]benzene (2). A solution of 3,5-bis(*tert*-butyldimethylsilyloxymethyl)phenylboronic acid (1.00 g, 2.44 mmol) (*21*) in THF/H_2O (5:1, 12 mL) was added to a solution of 1-iodobenzene (0.50 g, 2.44 mmol) and $PdCl_2$(dppf)·CH_2Cl_2 (dppf is 1,1′-bis(diphenylphosphanyl)ferrocene) (0.089 g, 0.122 mmol) in THF/H_2O (5:1, 12 mL). 2 M NaOH (3.66 mL) was added to the mixture, and the whole was stirred at 65 °C for 24 h. The reaction mixture was filtered through Celite pad. The eluant was partitioned between EtOAc and H_2O. The

organic layer was washed with aqueous $NaHCO_3$ (saturated) and brine, dried (Na_2SO_4), and concentrated. The residue was dissolved in THF (12.2 mL). TBAF (1 M in THF, 7.3 mL) was added to the solution, and the mixture was stirred at room temperature for 2 h. The solvent was evaporated in vacuo, and the resulting residue was purified by column chromatography (SiO_2, 2% MeOH in $CHCl_3$) to give **2** (0.486 g, 93%): ^{1}H NMR ($CDCl_3$) δ 7.61−7.34 (m, 8H), 4.77 (s, 4H), 1.84 (s, 2H). ^{13}C NMR (DMSO-d_6) δ 133.9, 133.2, 132.9, 120.3, 118.8, 118.5, 116.0, 116.0, 55.7. Anal. Calcd for $C_{14}H_{14}O_2$: C, 78.48; H, 6.59. Found: C, 78.29; H, 6.46.

*1-[3-(4,4′-Dimethoxytrityloxymethyl)-5-(hydroxymethyl)phenyl]benzene (**10**).* A mixture of **2** (0.48 g, 2.24 mmol) and DMTrCl (0.76 g, 2.24 mmol) in pyridine (11 mL) was stirred at room temperature for 4 h. The mixture was partitioned between EtOAc and aqueous $NaHCO_3$ (saturated). The organic layer was washed with brine, dried (Na_2SO_4), and concentrated. The residue was purified by column chromatography (SiO_2, 15−45% EtOAc in hexane) to give **10** (0.601 g, 52%): ^{1}H NMR ($CDCl_3$) δ 7.61−7.21 (m, 17H), 6.87−6.83 (m, 4H), 4.77 (d, 2H, J = 5.6), 4.25 (s, 2H), 3.79 (m, 6H). ^{13}C NMR ($CDCl_3$) δ 158.5, 145.0, 141.5. 141.4, 141.0, 140.2, 136.2, 130.1, 128.7, 128.2, 127.8, 127.3, 127.2, 126.7, 125.1, 124.6, 124.5, 113.1, 86.5, 65.6, 65.4, 60.4, 55.2. Anal. Calcd for $C_{35}H_{34}O_5 \cdot H_2O$: C, 78.63; H, 6.41. Found: C, 78.64; H, 6.16.

*1-[3-[[(2-Cyanoethoxy)(N,N-diisopropylamino)phosphanyl]oxymethyl]-5-(4,4′-dimethoxytrityloxymethyl)phenyl]benzene (**11**).* A mixture of **10** (0.42 g, 0.82 mmol), *N,N*-diisopropylethylamine (0.71 mL, 4.10 mmol), and chloro(2-cyanoethoxy)(*N,N*-diisopropylamino)phosphane (0.39 mL, 1.64 mmol) in THF (8 mL) was stirred at room temperature for 1 h. The mixture was partitioned between $CHCl_3$ and aqueous $NaHCO_3$ (saturated). The organic layer was washed with brine, dried (Na_2SO_4), and concentrated. The residue was purified by column chromatography (a neutralized SiO_2, EtOAc) to give **11** (0.52 g, 88%): ^{31}P NMR ($CDCl_3$) δ 149.0.

*1-[3,5-Bis(hydroxymethyl)phenyl]phenanthrene (**4**).* A solution of **7** in THF/H_2O (5:1, 12 mL) was added to a solution of 9-iodophenanthrene (0.74 g, 2.44 mmol) and $PdCl_2$(dppf)·CH_2Cl_2 (0.089 g, 0.122 mmol) in THF/H_2O (5:1, 12 mL). 2 M NaOH (3.66 mL) was added to the mixture, and the whole was stirred at 65 °C for 24 h. The reaction mixture was filtered through a Celite pad. The eluant was partitioned between EtOAc and H_2O. The organic layer was washed with aqueous $NaHCO_3$ (saturated) and brine, dried (Na_2SO_4), and concentrated. The residue was dissolved in THF (12.2 mL). TBAF (1 M in THF, 7.3 mL) was added to the solution, and the mixture was stirred at room temperature for 2 h. The solvent was evaporated in vacuo, and the resulting residue was purified by column chromatography (SiO_2, 2% MeOH in $CHCl_3$) to give **4** (0.47 g, 60%): ^{1}H NMR ($CDCl_3$) δ 8.76 (dd, 2H, J = 8.0 and 21.2), 7.89−7.87 (m, 2H), 7.70−7.48 (m, 8H), 4.82 (s, 4H), 1.80 (s, 2H). ^{13}C NMR ($CDCl_3$) δ 141.3, 140.9, 138.4, 131.4, 130.9, 130.5, 129.8, 128.5, 127.6, 127.3, 126.7, 126.6, 126.5, 126.4, 126.3, 124.4, 122.8, 122.4, 64.5. Anal. Calcd for $C_{22}H_{18}O_2 \cdot 1/5H_2O$: C, 83.10; H, 5.83. Found: C, 83.14; H, 5.86.

*1-[3-(4,4′-Dimethoxytrityloxymethyl)-5-(hydroxymethyl)phenyl]phenanthrene (**15**).* A mixture of **4** (0.46 g, 1.46 mmol) and DMTrCl (0.50 g, 1.46 mmol) in pyridine (7 mL) was stirred at room temperature for 3 h. The mixture was partitioned between EtOAc and aqueous $NaHCO_3$ (saturated). The organic layer was washed with brine, dried (Na_2SO_4), and concentrated. The residue was purified by column chromatography (SiO_2, 15−45% EtOAc in hexane) to give **15** (0.55 g, 61%): ^{1}H NMR ($CDCl_3$) δ 8.76 (dd, 2H, J = 8.0 and 22.0), 7.96−7.89 (m, 2H), 7.70−7.19 (m, 17H), 6.84−6.81 (m, 4H), 4.81 (s, 2H), 4.29 (s, 2H), 3.78 (m, 6H). ^{13}C NMR ($CDCl_3$) δ 158.4, 145.0, 141.0, 139.8, 138.5, 136.2, 131.5, 131.0, 130.6, 130.1, 129.9, 128.6, 128.2, 128.1, 127.8, 127.5, 127.4, 126.9, 126.8, 126.7, 126.6, 126.5, 126.4, 124.7, 122.9, 122.5, 113.1, 86.5, 65.6, 65.4, 55.2. Anal. Calcd for $C_{43}H_{36}O_4 \cdot 7/10H_2O$: C, 82.06; H, 5.99. Found: C, 82.04; H, 6.18.

*1-[3-[[(2-Cyanoethoxy)(N,N-diisopropylamino)phosphanyl]oxymethyl]-5-(4,4′-dimethoxytrityloxymethyl)phenyl]phenanthrene (**16**).* A mixture of **15** (0.35 g, 0.56 mmol), *N,N*-diisopropylethylamine (0.49 mL, 2.80 mmol), and chloro(2-cyanoethoxy)(*N,N*-diisopropylamino)phosphane (0.26 mL, 1.12 mmol) in THF (7 mL) was stirred at room temperature for 1 h. The mixture was partitioned between $CHCl_3$ and aqueous $NaHCO_3$ (saturated). The organic layer was washed with brine, dried (Na_2SO_4), and concentrated. The residue was purified by column chromatography (a neutralized SiO_2, EtOAc) to give **16** (0.34 g, 74%): ^{31}P NMR ($CDCl_3$) δ 149.0.

Solid Support Synthesis. A mixture of **10** (0.26 g, 0.50 mmol), succinic anhydride (0.15 g, 1.49 mmol), and DMAP (12 mg, 0.10 mmol) in pyridine (5 mL) was stirred at room temperature. After 24 h, the solution was partitioned between $CHCl_3$ and H_2O, and the organic layer was washed with H_2O and brine. The separated organic phase was dried (Na_2SO_4) and concentrated to give a succinate. Aminopropyl controlled pore glass (1.03 g, 0.12 mmol) was added to a solution of the succinate and EDCI (95 mg, 0.50 mmol) in DMF (12 mL), and the mixture was kept for 48 h at room temperature. After the resin was washed with pyridine, a capping solution (15 mL, 0.1 M DMAP in pyridine/Ac_2O = 9:1, v/v) was added and the whole mixture was kept for 24 h at room temperature. The resin was washed with MeOH and acetone, and dried in vacuo. The amount of loaded compound **10** to solid support was 49 μmol/g from calculation of released dimethoxytrityl cation by a solution of 70% $HClO_4$/EtOH (3:2, v/v). In a similar manner, solid support with **15** was obtained in 45 μmol/g loading amount.

RNA Synthesis. Synthesis was carried out with a DNA/RNA synthesizer by phosphoramidite method. Deprotection of bases and phosphates was performed in concentrated NH_4OH/EtOH (3:1, v/v) at room temperature for 12 h. 2′-TBDMS groups were removed by 1.0 M tetrabutylammonium fluoride (TBAF, Aldrich) in THF at room temperature for 12 h. The reaction was quenched with 0.1 M TEAA buffer (pH 7.0) and desalted on a Sep-Pak C18 cartridge. Deprotected ONs were purified by 20% PAGE containing 7 M urea to give the highly purified ON**45** (23), ON**46** (21), ON**47** (27), ON**48** (35), ON**49** (28), ON**50** (36), ON**51** (24), ON**52** (17), ON**53** (20), ON**54** (45), ON**57** (12), ON**58** (31), ON**59** (16), ON**60** (19), ON**63** (30), ON**64** (25), ON**65** (11), ON**66** (23), ON**69** (26), ON**70** (28), ON**71** (13), ON**74** (38), ON**75** (38), ON**76** (16), ON**77** (24), ON**78** (17), ON**79** (26). The yields are indicated in parentheses as OD units at 260 nm starting from 1.0 μmol scale. Extinction coefficients of the ONs were calculated from those of mononucleotides and dinucleotides according to the nearest-neighbor approximation method (*32*).

MALDI-TOF/MS Analysis of RNAs. Spectra were obtained with a time-of-flight mass spectrometer. ON**45**: calculated mass, 6443.9; observed mass, 6449.2. ON**46**: calculated mass, 6753.0; observed mass, 6751.8. ON**47**: calculated mass, 6543.9; observed mass, 6547.9. ON**48**: calculated mass, 6853.0; observed mass, 6853.2. ON**49**: calculated mass, 6644.0; observed mass, 6646.4. ON**50**: calculated mass, 6953.1; observed mass, 6951.0. ON**51**: calculated mass, 6696.0; observed mass, 6693.1. ON**52**: calculated mass, 7005.1; observed mass, 7004.8. ON**53**: calculated mass, 7067.0; observed mass, 7065.5. ON**54**: calculated mass, 7011.0; observed mass, 7007.9. ON**57**: calculated mass, 6859.2; observed mass, 6852.0. ON**58**: calculated mass, 6909.0; observed mass, 6902.4. ON**59**: calculated mass, 7008.3; observed mass, 7004.9. ON**60**: calculated mass, 7058.4; observed

mass, 7052.4. ON**63**: calculated mass, 6641.9; observed mass, 6645.5. ON**64**: calculated mass, 6688.0; observed mass, 6685.9. ON**65**: calculated mass, 6814.0; observed mass, 6820.1. ON**66**: calculated mass, 6522.9; observed mass, 6526.2. ON**69**: calculated mass, 6745.9; observed mass, 6746.1. ON**70**: calculated mass, 6568.9; observed mass, 6565.5. ON**71**: calculated mass, 6695.0; observed mass, 6696.0. ON**74**: calculated mass, 6739.9; observed mass, 6739.0. ON**75**: calculated mass, 6802.9; observed mass, 6801.4. ON**76**: calculated mass, 7066.0; observed mass, 7061.8. ON**77**: calculated mass, 6929.0; observed mass, 6933.2. ON**78**: calculated mass, 7066.0; observed mass, 7067.1. ON**79**: calculated mass, 6929.0; observed mass, 6931.6.

Thermal Denaturation Study. Each solution containing each siRNA (3 μM) in a buffer composed of 10 mM Na_2HPO_4/NaH_2PO_4 (pH 7.0) and 100 mM NaCl was heated at 95 °C for 3 min, then cooled gradually to an appropriate temperature, and used for the thermal denaturation studies. Thermally induced transitions of each mixture were monitored at 260 nm with a spectrophotometer.

Dual-Luciferase Assay. HeLa cells were grown at 37 °C in a humidified atmosphere of 5% CO_2 in air in Minimum Essential Medium (MEM) (Invitrogen) supplemented with 10% fetal bovine serum (FBS). Twenty-four hours before transfection, HeLa cells (4×10^4/mL) were transferred to 96-well plates (100 μL per well). They were transfected, using TransFast (Promega), according to instructions for transfection of adherent cell lines. Cells in each well were transfected with a solution (35 μL) of 20 ng of psiCHECK-2 vector (Promega), the indicated amounts of siRNAs, and 0.3 μg of TransFast in Opti-MEM I Reduced-Serum Medium (Invitrogen), and incubated at 37 °C. Transfection without siRNA was used as a control. After 1 h, MEM (100 μL) containing 10% FBS and antibiotics was added to each well, and the whole was further incubated at 37 °C. After 24 h, cell extracts were prepared in Passive Lysis Buffer (Promega). Activities of firefly and *Renilla* luciferases in cell lysates were determined with a dual-luciferase assay system (Promega) according to a manufacturer's protocol. The results were confirmed by at least three independent transfection experiments with two cultures each and are expressed as the average from four experiments as mean ± SD.

Partial Hydrolysis of ONs with Snake Venom Phosphodiesterase. Each ON (300 pmol) labeled with fluorescein at the 5′-end was incubated with snake venom phosphodiesterase (3 ng) in a buffer containing 37.5 mM Tris-HCl (pH 7.0) and 7.5 mM $MgCl_2$ (total 100 μL) at 37 °C. At appropriate periods, aliquots (5 μL) of the reaction mixture were separated and added to a solution of 9 M urea (15 μL). The mixtures were analyzed by electrophoresis on 20% polyacrylamide gel containing 7 M urea. The labeled ON in the gel was visualized by a Typhoon system (Amersham Biosciences).

Stability of siRNAs in the PBS Containing Bovine Serum. Each siRNA (600 pmol) labeled with fluorescein at the 5′-end of a sense strand was incubated in PBS (300 μL) containing 40% bovine serum at 37 °C. At appropriate periods, aliquots (5 μL) of the reaction mixture were separated and added to a loading solution (15 μL), and then the whole was immediately frozen in dry ice. The mixtures were analyzed by electrophoresis on 20% polyacrylamide gel under nondenaturing conditions. The labeled siRNA in the gel was visualized by a Typhoon system (Amersham Biosciences).

Subgenomic HCV Replicon Cells. Subgenomic HCV replicon cells (R6FLR-N) were conditional expression system of the HCV-nonstructure region and luciferase gene. These cells were cultured in DMEM-GlutaMAX High glucose (GIBCO) supplemented with 10% FBS, 1 unit penicillin (GIBCO), 100 μg/mL streptomycin (GIBCO), and 500 μg/mL G418 (GIBCO).

Transfection and Evaluation of Virus Replication. The subgenomic HCV replicon cells (R6FLR-N) were transfected with the siRNAs by reverse transfection. The cells were plated in 96-well plate (Falcon) at a density of 4×10^3 cells/well. Each siRNA (100 aM − 1 nM) was transfected to the cells using Lipofectamine RNAiMAX (Invitrogen) and Opti-MEM (GIBCO-BRL). The cells were incubated for 72 h after being transfected with siRNAs. HCV replication was evaluated by luminescence in a Mithras LB940 (Berthold Technologies, Wildbad, Germany) using Bright-Glo Luciferase Assay System (Promega) according to the manufacturer's protocol.

Cell Viability. In order to evaluate cytotoxic effects of the siRNAs, cell viabilities were measured by metabolic conversion of 2-(2-methoxy-4-nitrophenyl)-3-(4-nitrophenyl)-5-(2,4-disulfophenyl)-2*H*-tetrazolium, monosodium salt (WST-8) using a Cell Counting Kit-8 (Dojindo, Kumamoto, Japan) according to the manufactuer's protocol.

ACKNOWLEDGMENT

This study was supported in part by a Grant-in-Aid from Precursory Research for Embryonic Science and Technology (PRESTO) of Japan Science and Technology (JST) and a Grant-in-Aid for Scientific Research (C) from Japan Society for the Promotion of Science (JSPS) to Y.U. We are also grateful to Dr. Y. Kitamura (Gifu University) for providing technical assistance.

LITERATURE CITED

(1) Fire, A., Xu, S., Montgomery, M. K., Kostas, S. A., Driver, S. E., and Mello, C. C. (1998) Potent and specific genetic interference by double-stranded RNA in *Caenorhabditis elegans*. *Nature 391*, 806–811.

(2) Elbashir, S. M., Harborth, J., Lendeckel, W., Yalcin, A., Weber, K., and Tuschl, T. (2001) Duplexes of 21-nucleotide RNAs mediate RNA interference in cultured mammalian cells. *Nature 411*, 494–498.

(3) Elbashir, S. M., Lendeckel, W., and Tuschl, T. (2001) RNA interference is mediated by 21- and 22nucleotide RNAs. *Genes Dev. 15*, 188–200.

(4) Bumcrot, D., Manoharan, M., Koteliansky, V., and Sah, D. W. Y. (2006) RNAi therapeutics: a potential new class of pharmaceutical drugs. *Nat. Chem. Biol. 2*, 711–719.

(5) Behlke, M. A. (2006) Progress toward *in vivo* use of siRNAs. *Mol. Ther. 13*, 644–670.

(6) Kim, D. A., and Rossi, J. J. (2007) Strategies for silencing human disease using RNA interference. *Nat. Rev. Genet. 8*, 173–184.

(7) Schwarz, D. S., Hutvágner, G., Du, T., Xu, Z., Aronin, N., and Zamore, P. D. (2003) Asymmetry in the assembly of the RNAi enzyme complex. *Cell 115*, 199–208.

(8) Khvorova, A., Reynolds, A., and Jayasena, S. D. (2003) Functional siRNAs and miRNAsexhibit strand bias. *Cell 115*, 209–216.

(9) Tomari, Y., Matranga, C., Haley, B., Martinez, N., and Zamore, P. D. (2004) A protein sensor for siRNA asymmetry. *Science 306*, 1377–1380.

(10) Steiner, F. A., Hoogstrate, S. W., Okihara, K. L., Thijssen, K. L., Ketting, R. F., Plasterk, R. H. A., and Sijen, T. (2007) Structural features of small RNA precursors determine Argonaute loading in *Caenorhabditis elegans*. *Nat. Struct. Mol. Biol. 14*, 927–933.

(11) Mi, S., Cai, T., Hu, Y., Chen, Y., Hodges, E., Ni, F., Wu, L., Li, S., Zhou, H., Long, C., Chen, S., Hannon, G. J., and Qi, Y. (2008) Sorting of small RNAs into *Arabidopsis* Argonate complexes is directed by the 5′ terminal nucleotide. *Cell 133*, 116–127.

(12) Kawamata, T., Seitz, H., and Tomari, Y. (2009) Structural determinants of miRNAs for RISC loading and slicer-independent unwinding. *Nat. Struct. Mol. Biol. 16*, 953–960.
(13) Yoda, M., Kawamata, T., Paroo, Z., Ye, X., Iwasaki, S., Liu, Q., and Tomari, Y. (2010) ATP-dependent human RISC assembly pathways. *Nat. Struct. Mol. Biol. 16*, 17–23.
(14) Ghildiyal, M., Xu, J., Seitz, H., Weng, Z., and Zamore, P. D. (2010) Sorting of *Drosophila* small silencing RNAs partitions microRNA* strands into the RNA interference pathway. *RNA 16*, 43–56.
(15) Chen, P. Y., Weinmann, L., Gaidatzis, D., Pei, Y., Zavolan, M., Tuschl, T., and Meister, G. (2008) Strand-specific 5′-O-methylation of siRNA duplexes controls guide strand selection and targeting specificity. *RNA 14*, 263–274.
(16) Parker, J. S., Roe, S. M., and Barford, D. (2005) Structure insights into mRNA recognition from a PIWI domain-siRNA guide complex. *Nature 434*, 663–666.
(17) Ma, J.-B., Yuan, Y.-R., Meister, G., Pei, Y., Tuschl, T., and Patel, D. J. (2005) Structure basis for 5′-end-specific recognition of guide RNA by the *A. fulgidus* Piwi protein. *Nature 434*, 666–670.
(18) Wang, Y., Sheng, G., Juranek, S., Tuschl, T., and Patel, D. J. (2008) Structure of the guide-strand-containing argonaute silencing complex. *Nature 456*, 209–213.
(19) Wang, Y., Juranek, S., Li, H., Sheng, G., Tuschl, T., and Patel, D. J. (2008) Structure of an argonaute silencing complex with a seed-containing guide DNA and target RNA duplex. *Nature 456*, 921–926.
(20) Wang, Y., Juranek, S., Li, H., Sheng, G., Wardle, G. S., Tuschl, T., and Patel, D. J. (2010) Nucleation, propagation and cleavage of target RNAs in Ago silencing complexes. *Nature 461*, 754–761.
(21) Ueno, Y., Komatsuzaki, S., Takasu, K., Kawai, S., Kitamura, Y., and Kitade, Y. (2009) Synthesis and properties of oligonucleotides containing novel fluorescent biaryl units. *Eur. J. Org. Chem. 28*, 4763–4769.
(22) Ueno, Y., Watanabe, Y., Shibata, A., Yoshikawa, K., Takano, T., Kohara, M., and Kitade, Y. (2009) Synthesis of nuclease-resistant siRNAs possessing universal overhangs. *Bioorg. Med. Chem. 17*, 1974–1981.
(23) Lingel, A., Simon, B., Izaurralde, E., and Sattler, M. (2003) Structure and nucleic-acid binding of the *Drosophila* Argonaute 2 PAZ domain. *Nature 426*, 465–469.
(24) Yan, K. S., Yan, S., Farooq, A., Han, A., Zeng, L., and Zhou, M.-M. (2003) Structure and conserved RNA binding of the PAZ domain. *Nature 426*, 469–474.
(25) Song, J.-J., Liu, J., Tolia, N. H., Schneiderman, J., Smith, S. K., Martienssen, R. A., Hannon, G. J., and Joshua-Tor, L. (2003) The crystal structure of the Argonaute2 PAZ domain reveals an RNA binding motif in RNAi effector complexes. *Nat. Struct. Biol. 12*, 1026–1032.
(26) Ma, J.-B., Te, K., and Patel, D. J. (2004) Structure basis for overhang-specific small interfering RNA recognition by the PAZ domain. *Nature 429*, 318–322.
(27) Somoza, Á., Terrazas, M., and Eritja, R. (2010) Modified siRNAs for the study of the PAZ domain. *Chem. Commun. 46*, 4270–4272.
(28) Qiu, S., Adema, C. M., and Lane, T. (2005) A computational study of off-target effects of RNA interference. *Nucleic Acids. Res. 33*, 1834–1847.
(29) Jackson, A. L., Burchard, J., Schelter, J., Chau, B. N., Cleary, M., Lim, L., and Linsley, P. S. (2006) Widespread siRNA "off-target" transcript silencing mediated by seed region sequence complementarity. *RNA 12*, 1179–1187.
(30) Watanabe, T., Sudoh, M., Miyagishi, M., Akashi, H., Arai, M., Inoue, K., Taira, K., Yoshida, M., and Kohara, M. (2006) Intracellular-diced dsRNA has enhanced efficacy for silencing HCV RNA and overcomes variation in the viral genotype. *Gene Ther. 13*, 883–892.
(31) Uhlmann, E., Vollmer, J., and Krieg, A. M. (2010) Nucleic acid-lipophilic conjugates. U.S. Patent Appl. US 20100183639A1.
(32) Puglisi, J. D., and Tinoco, I., Jr. (1989) *In Methods in Enzymology*, Dahlberg, J. E., and Abelson, J. N., Eds.; pp 304–325, Vol 180, Academic Press, Inc., San Diego.

BC100301W

Exp. Anim. 60(2), 93–100, 2011

—Review—
Review Series: Frontiers of Model Animals for Human Diseases

An Experimental Mouse Model for Hepatitis C Virus

Kiminori KIMURA[1,2] and Michinori KOHARA[1]

[1]*Department of Microbiology and Cell Biology, Tokyo Metropolitan Institute of Medical Science, Tokyo 156-8506 and* [2]*Division of Hepatology, Tokyo Metropolitan Cancer and Infectious Diseases Center, Komagome Hospital, Tokyo 113-8677, Japan*

Abstract: Chronic hepatitis C virus (HCV) infection affects approximately 170 million people and is a major global health problem because infected individuals can develop liver cirrhosis and hepatocellular carcinoma. Despite significant improvements in antiviral drugs, only around 50% of treated patients with genotype 1 and 4 demonstrate HCV clearance. Unfortunately, an anti-HCV vaccine is still not available. To progress treatment of HCV, it is necessary to understand the mechanism(s) by which HCV infects hepatocytes, and how the host immune response prevents the spread of the virus. Because HCV infects only humans and chimpanzees, it is difficult to evaluate immune response mechanisms, and the effects of chemicals and new technologies on these response mechanisms. These difficulties underline the importance of establishing a small HCV-infected animal model. This review focuses on the progress made in recent years towards the development of an experimental mouse model for HCV.

Key words: apoptosis, B cell lymphoma, HCV, immune response, transgenic mice

Introduction

Hepatitis C virus (HCV) is a non-cytopathic, hepatotropic member of the *Flaviviridae* family, causing acute and chronic necroinflammatory liver diseases [25]. Chronic HCV infection has caused an epidemic with approximately 170 million people infected worldwide and three to four million people newly infected each year [25, 35]. Natural history studies show that 5–20% of patients develop cirrhosis after about 20 years of infection [1, 42, 49]. An increasing number of patients with cirrhosis will develop hepatocellular carcinoma. End-stage liver disease due to chronic HCV infection is the leading cause of liver transplantation in the western world [36]. Furthermore, co-infection with HCV and human immunodeficiency virus (HIV) results in more serious liver cirrhosis than HCV infection alone and the mortality of HIV-infected HCV patients is a serious problem in the USA [44. 55].

The HCV genome is a 9.6-kb, uncapped, linear, single-strand RNA molecule with positive polarity that serves as a template for both translation and replication. Translation of the plus-strand RNA initiates at an internal ribosomal entry site, resulting in the production of a single polyprotein precursor that is processed into structural (C, E1, E2, p7) and non-structural (NS2, NS3, NS4A, NS4B, NS5A, and NS5B) protein subunits by host and viral proteases [8, 9, 37, 46]. Because of the lack of a proofreading func-

(Received 20 December 2010 / Accepted 29 January 2010)
Address corresponding: M. Kohara, Department of Microbiology and Cell Biology, Tokyo Metropolitan Institute of Medical Science, 2–1–6 Kamikitazawa, Setagaya-ku, Tokyo 156-8506, Japan

tion for the RNA-dependent RNA-polymerase (NS5B), HCV has a high mutation rate and exists as a genetically heterogeneous quasispecies in individual patients [8].

It is well established that the pathogenesis of HCV infection is controlled by host-virus interactions mediated by the immune response [4, 5, 13]. It has been difficult to clarify the relationship between HCV and the host immune response because of the fact that HCV is only infectious in humans and chimpanzees [3, 11]. It has also been demonstrated that viral clearance during self-limited acute HCV infection is characterized by a vigorous, polyclonal CD4 and CD8 T-cell response [6, 12, 29, 38, 43]. However, the lack of activity in inducing an effective antigen-specific CD4 and CD8 T-cell response in chronically infected HCV cases has been studied in chimpanzees [50], and also in humans infected via needle stick accidents [47]. These studies suggest that a poor immunological response to HCV probably leads to persistent infection. Failure to effectively produce antigen-specific T-cells is possibly the result of viral overload [15–17] and the high level of regulatory T cells present [40]. However, it remains unknown why HCV infection causes persistent infection. It has also been demonstrated that viral replication is inhibited by antigen-specific T cells as well as natural killer (NK) cells, natural killer T (NKT) cells and macrophages in the liver of hepatitis B virus (HBV) transgenic mice [18, 21, 22], indicating that viral clearance requires innate and acquired immune responses.

In this review, we describe an experimental mouse model for HCV infection which allows us to analyze the mechanisms of chronic persistent infection.

HCV Transgenic Mice Models

Generation of HCV transgenic mice using the Cre/loxp switching system

A transgenic mouse model using a stable expression system generates immunotolerance to transgene products. Therefore, an HCV protein switching expression system may be suitable for *in vivo* assays of HCV protein effects, as HCV is thought to infect humans with a mature immune function [1]. Using the *Cre/loxP* system, we developed a transgenic mouse model with efficient conditional transgene activation of HCV cDNA (core, E1, E2, and NS2) (Fig. 1), and two transgenic lines, CN2-8 and CN2-29, were generated [48]. The *Cre/loxP* system has been used in combination with a recombinant adenovirus vector expressing Cre to alter gene expression in the livers of transgenic mice [34]. Temporal control of viral gene expression using a conditional transgene activation system enables detailed analysis of the immune responses in the host, and observation of cytopathic effects due to viral proteins. HCV proteins were mainly detected in the livers of conditionally expressing transgenic mice. Efficient recombination was observed in transgenic mice livers upon intravenous administration of adenoviruses expressing Cre DNA recombinase. After transgene activation, most hepatocytes were stained with anti-core polyclonal antibody, and 21-, 37-, and 64-kDa proteins were detected by western blot analysis in liver lysates using anti-core, -E1, and -E2 monoclonal antibodies, respectively. Serum core protein was detected in transgenic mice 7 days after transgene activation with concurrent increases in serum alanine aminotransferase levels. Importantly, we observed no significant histopathological changes between infected and uninfected CN2 transgenic mice when CD4- and CD8-positive cells were depleted in the infected mice (Fig. 2). These results suggest that HCV structural proteins are not strongly cytopathic to hepatocytes in the absence of an immune response.

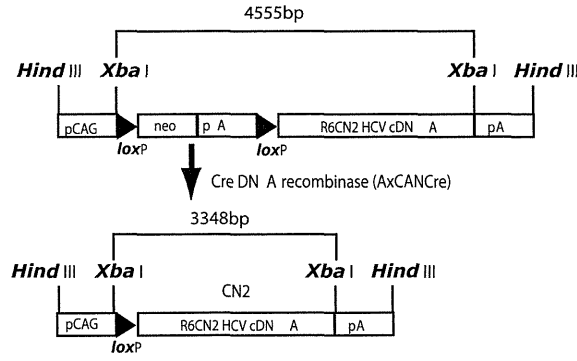

Fig. 1. Structure of CALNCN2, the Cre-mediated activation transgene unit. R6CN2 HCV cDNA (nucleotides 294–3435) was cloned downstream of the CAG promoter, neomycin-resistant gene (neo) and poly(A) signal that was flanked by two *loxP* sequences. R6CN2 HCV cDNA contains the core, E1, E2, and NS2 regions.

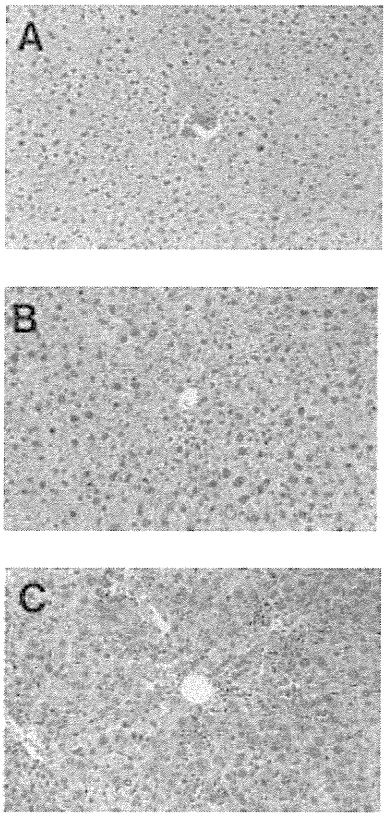

Fig. 2. Histopathology of livers of HCV Tg mice. A, uninfected CN2-8 mouse. B, $CD4^+$ and $CD8^+$ cell-depleted CN2-8 mouse infected with AxCANCre and analyzed at day 7. C, CN2-8 mouse infected with AxCANCre and analyzed at day 7. (×250 magnification).

HCV transgenic mice are resistant to Fas antibody-mediated lethality

The role of apoptosis in HCV infection is not well defined. Furthermore, the kinetics and extent of hepatocyte apoptosis as well as the pro- and anti-apoptotic mechanisms involved remain unclear. We demonstrated that transgene expression in HCV transgenic mice causes resistance to Fas antibody-stimulated lethality [27]. Apoptotic cell death in the livers of HCV protein-expressing mice was significantly reduced compared to non-expressing mice. Histopathological analysis and DNA fragmentation analysis revealed that the HCV proteins suppressed *Fas*-mediated apoptotic cell death. To identify the target pathway of HCV proteins, we characterized caspase activity and showed that the activation of caspase-9 and caspase-3/7, but not caspase-8, was inhibited by HCV proteins. In addition, cytochrome *c* release from mitochondria was inhibited in HCV protein-expressing mice. These results indicate that the expression of HCV proteins may have directly or indirectly inhibited Fas-mediated apoptosis and cell death in mice by repressing the release of cytochrome *c* from mitochondria, thereby suppressing caspase-9 and caspase-3/7 activation. Furthermore, HCV might cause persistent infection as a result of suppression of *Fas*-mediated cell death and inhibition of HCV-infected hepatocyte rejection in the liver, given that numerous viruses have been reported to evade apoptotic mechanisms resulting persistent infection [23].

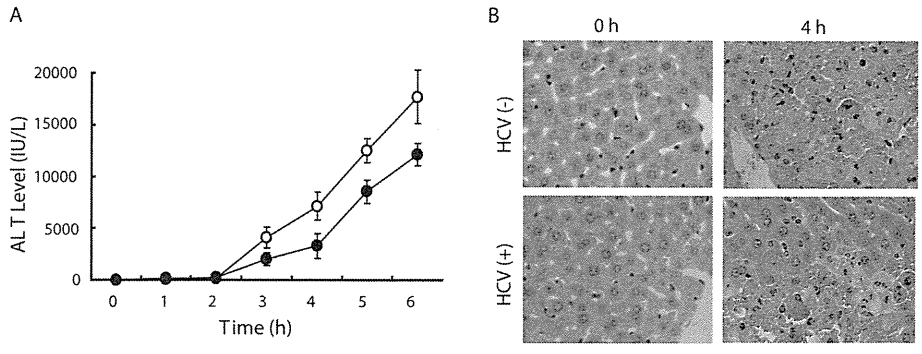

Fig. 3. Serum ALT level and histological analysis of livers after anti-Fas antibody administration. A, serum ALT levels of anti-Fas antibody-injected HCV non-expressing (*open circles*) and expressing (*closed circle*) mice. ALT levels are expressed as the mean ± SD of three individual experiments. B, hematoxylin and eosin staining of liver sections from transgenic mice at pretreatment and 4 h after anti-Fas antibody injection.